

Search for 100 MeV to 10 GeV γ -ray lines in the *Fermi*-LAT data and implications for gravitino dark matter in the $\mu\nu$ SSM

**Andrea Albert,^a Germán A. Gómez-Vargas,^{b,c,d} Michael Grefe,^{e,b}
Carlos Muñoz,^b Christoph Weniger,^f Elliott D. Bloom,^a
Eric Charles,^a Mario N. Mazziotta,^g and Aldo Morselli^d**

^aW. W. Hansen Experimental Physics Laboratory, Kavli Institute for Particle Astrophysics and Cosmology, Department of Physics and SLAC National Accelerator Laboratory, Stanford University, Stanford, CA 94305, USA

^bInstituto de Física Teórica UAM/CSIC and Departamento de Física Teórica, Universidad Autónoma de Madrid, Cantoblanco, E-28049 Madrid, Spain

^cSince 1st January 2014 at: Instituto de Física, Pontificia Universidad Católica de Chile, Avenida Vicuña Mackenna 4860, Santiago, Chile

^dIstituto Nazionale di Fisica Nucleare, Sezione di Roma “Tor Vergata”, I-00133 Roma, Italy

^eInstitut für Theoretische Physik, Universität Hamburg, Luruper Chaussee 149, D-22761 Hamburg, Germany

^fGRAPPA, University of Amsterdam, Science Park 904, 1098XH Amsterdam, Netherlands

^gIstituto Nazionale di Fisica Nucleare, Sezione di Bari, I-70126 Bari, Italy

E-mail: aalbert@slac.stanford.edu, ggomezv@uc.cl, michael.grefe@desy.de,
carlos.munoz@uam.es, c.weniger@uva.nl, elliott@slac.stanford.edu,
echarles@slac.stanford.edu, marionicola.mazziotto@ba.infn.it,
aldo.morselli@roma2.infn.it.

Abstract. Dark matter decay or annihilation may produce monochromatic signals in the γ -ray energy range. In this work we argue that there are strong theoretical motivations for studying these signals in the framework of gravitino dark matter decay and we perform a search for γ -ray spectral lines from 100 MeV to 10 GeV with *Fermi*-LAT data. In contrast to previous line searches at higher energies, the sensitivity of the present search is dominated by systematic uncertainties across most of the energy range considered. We estimate the size of systematic effects by analysing the flux from a number of control regions, and include the systematic uncertainties consistently in our fitting procedure. We have not observed any significant signals and present model-independent limits on γ -ray line emission from decaying and annihilating dark matter. We apply the former limits to the case of the gravitino, a well-known dark matter candidate in supersymmetric scenarios. In particular, the R -parity violating “ μ from ν ” Supersymmetric Standard Model ($\mu\nu$ SSM) is an attractive scenario in which including right-handed neutrinos solves the μ problem of the Minimal Supersymmetric Standard Model while simultaneously explaining the origin of neutrino masses. At the same time, the violation of R -parity renders the gravitino unstable and subject to decay into a photon and a neutrino. As a consequence of the limits on line emission, $\mu\nu$ SSM gravitinos with masses larger than about 5 GeV, or lifetimes smaller than about 10^{28} s, are excluded at 95% confidence level as dark matter candidates.

Keywords: dark matter experiments, gamma ray experiments, dark matter theory

1 Introduction

The existence of non-baryonic cold dark matter (DM) in the Universe, which today is confirmed by a large number of observations from galactic [1] to cosmological scales [2], is arguably the most compelling and striking evidence for physics outside the realm of the Standard Model of particle physics (SM) [3–5]. Many extensions to the SM contain long-lived particles that are attractive candidates for DM. Typically the focus is on weakly interacting massive particles (WIMPs) like Kaluza–Klein DM [6, 7], supersymmetric neutralinos [3–5] or right-handed sneutrinos [8, 9], but non-WIMP candidates like gravitinos in R -parity violating models such as the “ μ from ν ” Supersymmetric Standard Model ($\mu\nu$ SSM) may also constitute some, if not all of the DM [10]. These DM candidate particles may be observed indirectly via their annihilation (in the case of WIMPs) or decay (as for gravitinos) into SM particles, in particular γ rays.

These γ rays may be detected by the Large Area Telescope (LAT) on board the *Fermi* Gamma-ray Space Telescope (*Fermi*) [11], which is exploring the γ -ray sky in the energy range 20 MeV to above 300 GeV. We typically expect most of the DM-induced γ -ray emission to have a broad spectrum, which can be difficult to disentangle from astrophysical diffuse γ -ray backgrounds. For a recent review of indirect DM searches with γ rays see ref. [12]. However, spectral lines can be produced by the two-body decay or annihilation of DM particles into final states that include γ rays. Several searches have been performed using *Fermi*-LAT data for such spectral lines [13–17]. Typically these analyses have focused on searches for lines above a few GeV, since WIMPs are expected to be heavy ($\gtrsim 10$ GeV). We perform a search

for lines below those energies, where the statistical errors become very small and systematic uncertainties dominate. In this paper we argue that there are strong theoretical motivations to search for spectral lines from lower-mass gravitino decays. We also discuss the systematic uncertainties and how we incorporated them into our final results.

By far the best studied and most popular extension of the SM is the Minimal Supersymmetric Standard Model (MSSM) [18]. For example the MSSM solves the hierarchy problem that causes scalar masses to diverge in the SM. Also, although the LHC experiments have yet to find evidence of new particles predicted in the MSSM, we expect to learn more when it turns back on in 2015 and reaches 14 TeV. Furthermore, if R -parity is conserved, the lightest neutralino of the MSSM is a viable and well-known candidate for WIMP DM. However, the MSSM has the so-called μ problem [19]. This arises from the requirement of a supersymmetric mass term for the Higgs bosons in the superpotential, $\mu \hat{H}_u \hat{H}_d$, where \hat{H}_u and \hat{H}_d are the up and down Higgs-doublet superfields, respectively. This bilinear term is necessary, for example, to generate Higgsino masses in order to fulfil the current experimental bounds on chargino masses, which imply $\mu \gtrsim 100$ GeV. However, the existence of a Grand Unified Theory (GUT) and/or a gravitational theory with typical scales 10^{16} and 10^{19} GeV, respectively, would require an explanation of how to obtain a small supersymmetric mass, $\mu \sim 1$ TeV, which is necessary in order to reproduce the correct electroweak symmetry breaking without fine tuning.

The $\mu\nu$ SSM [20] provides a solution to the μ problem through mixing terms in the superpotential between the three right-handed neutrino superfields, $\hat{\nu}_i^c$, and the Higgs superfields, $\lambda_i \hat{\nu}_i^c \hat{H}_d \hat{H}_u$. These produce an effective μ term¹ when the electroweak symmetry is broken and the sneutrinos acquire vacuum expectation values, $\mu = \lambda_i \langle \tilde{\nu}_i^c \rangle$. On the other hand, mixing terms among right-handed neutrinos, $\kappa_{ijk} \hat{\nu}_i^c \hat{\nu}_j^c \hat{\nu}_k^c$, contribute to generate effective Majorana masses for neutrinos at the electroweak scale, $\sim \kappa_{ijk} \langle \tilde{\nu}_k^c \rangle$. With neutrino Yukawa couplings $Y_\nu \lesssim 10^{-6}$, this dynamically generated electroweak-scale seesaw mechanism can easily reproduce current measurements of neutrino mass differences and mixing angles [21–25]. Given that the $\mu\nu$ SSM is a well motivated and attractive model, its phenomenology at the LHC has been analysed in several works [22, 23, 25–30]. Cosmological issues in this model have also been considered, and in particular the generation of the baryon asymmetry of the Universe was studied in detail [31, 32], with the interesting result that electroweak baryogenesis can be realised [31] while thermal leptogenesis is disfavoured in the context of the $\mu\nu$ SSM [32].

The mixing terms characterising the $\mu\nu$ SSM produce an explicit breaking of R -parity. The size of the breaking is small, since it is determined by Y_ν . As a consequence of the R -parity violation, the lightest supersymmetric particle (LSP) is no longer stable. Thus, the lightest neutralino/sneutrino would have a very short lifetime and could not be a viable DM candidate. Nevertheless, if the role of the LSP is played by the gravitino, its decay is suppressed both by the feebleness of the gravitational interaction and by the small R -parity violating coupling, and, as a consequence, its lifetime can be much longer than the age of the Universe. In addition, the gravitino can be produced by thermal scatterings in the early Universe with a relic density matching the observed DM density in the Universe. Thus, the gravitino, which is a superweakly interacting massive particle (superWIMP), represents a

¹In the $\mu\nu$ SSM, the usual μ term of the MSSM is absent from the superpotential, and only dimensionless trilinear couplings are present. This can be achieved by the presence of a Z_3 symmetry. Let us emphasise that this is actually what happens in superstring constructions, where the low-energy limit is determined by the massless superstring modes. Since the massive modes have huge masses, of the order of the string scale, only the trilinear couplings for the massless modes are relevant.

good DM candidate. Most importantly, as pointed out in ref. [33] for the case of R -parity violation, gravitino decays in the Milky Way halo would produce monochromatic γ rays with an energy equal to half of the gravitino mass, and therefore its presence can, in principle, be inferred indirectly from γ -ray observations.²

Several searches for DM-induced γ -ray lines have been performed using *Fermi*-LAT data. One of the first explicit searches for γ -ray lines from gravitino DM in the $\mu\nu$ SSM was performed in [10]. From the non-observation of prominent sharp features in the diffuse emission measurement (based on 5 months of data) reported by the *Fermi*-LAT collaboration [41], gravitinos with masses larger than 10 GeV turn out to be disfavoured, as well as lifetimes smaller than about 3 to 5×10^{27} s. In ref. [14], 2 years of *Fermi*-LAT data were used to constrain γ -ray lines in the energy range between 1 GeV and 300 GeV. Stringent lower bounds on the gravitino lifetime of about 5×10^{28} s were obtained for masses above 2 GeV. When these bounds are applied to the $\mu\nu$ SSM, they imply that the gravitino mass must be smaller than 4 GeV [42]. At somewhat lower energies, limits have also been established from observations of the Galactic Centre by the Energetic Gamma Ray Experiment Telescope (EGRET) on board the *Compton Gamma Ray Observatory* [43]. In refs. [13, 15, 16], the *Fermi*-LAT collaboration presented constraints on monochromatic γ -ray emission. In particular, in ref. [16] using 44 months of data, the derived limits refer to the emission above 5 GeV, covering, in the context of gravitino DM, masses larger than 10 GeV. As we will show, this limit implies that gravitinos with masses larger than 10 GeV are excluded in the $\mu\nu$ SSM.

Given these previous results, and the interest of the $\mu\nu$ SSM as an attractive supersymmetric model that will be tested at the LHC, an extension of the analyses, covering line energies below a few GeV, is of great importance. In this work we report on a search for γ -ray spectral lines from 100 MeV to 10 GeV using 62 months of *Fermi*-LAT data. In this energy range, because of the small statistical uncertainties, the analysis is dominated by systematic effects that may fake or mask a line signal. Therefore, for the first time, we present γ -ray line limits where systematic uncertainties are included in the likelihood fitting and the calculation of limits.

This work is organised as follows. In section 2, gravitino DM in the $\mu\nu$ SSM is introduced, paying special attention to its lifetime and associated relic density. In section 3, after discussing the DM distribution we adopted as a baseline for this analysis, we concentrate on the data analysis and our treatment of systematic uncertainties and derive constraints on the parameter space of both generic decaying and annihilating DM. Finally, in section 4 the constraints on decaying DM are applied to the $\mu\nu$ SSM gravitino DM model and our results are compared with previous limits reported in the literature. The conclusions are left for section 5.

2 Gravitino dark matter in the $\mu\nu$ SSM

2.1 Gravitino lifetime

In the supergravity Lagrangian there is an interaction term between the gravitino, $\Psi_{3/2}$, the field strength for the photon, and the photino. Due to the breaking of R -parity, the

²The γ -ray line signature from gravitino DM decay is not an exclusive feature of the $\mu\nu$ SSM. Other gravitino DM scenarios with bilinear or trilinear R -parity violation as discussed in refs. [34–37] may exhibit the same decay signature [38]. In addition, this signature also appears in models with axino DM decay via bilinear R -parity violation [39, 40]. The γ -ray line constraints derived in this work thus could also be applied to constrain those models.

photino and the left-handed neutrinos are mixed, and thus the gravitino will be able to decay, through the interaction term, into a photon and a neutrino with energies equal to half of the gravitino mass, $m_{3/2}$ [33].³ Therefore, the presence of the gravitino can, in principle, be inferred indirectly from observations of the diffuse backgrounds of photons or neutrinos.⁴

The lifetime of the gravitino LSP in the $\mu\nu$ SSM is typically much longer than the age of the Universe, making it a viable DM candidate. From the supergravity Lagrangian one obtains a decay width, Γ , given by [33]

$$\Gamma \left(\Psi_{3/2} \rightarrow \sum_i \gamma \nu_i \right) \simeq \frac{1}{32\pi} |U_{\tilde{\gamma}\nu}|^2 \frac{m_{3/2}^3}{M_P^2}, \quad (2.1)$$

where $M_P = 2.4 \times 10^{18}$ GeV is the reduced Planck mass, and $|U_{\tilde{\gamma}\nu}|^2$ determines the neutrino content of the photino:

$$|U_{\tilde{\gamma}\nu}|^2 = \sum_{i=1}^3 |N_{i1} \cos \theta_W + N_{i2} \sin \theta_W|^2. \quad (2.2)$$

Here N_{i1} (N_{i2}) is the Bino (Wino) component of the i -th neutrino, and θ_W is the weak mixing angle. The gravitino lifetime can then be written as:

$$\tau_{3/2} \simeq 3.8 \times 10^{27} \text{ s} \left(\frac{|U_{\tilde{\gamma}\nu}|^2}{10^{-16}} \right)^{-1} \left(\frac{m_{3/2}}{10 \text{ GeV}} \right)^{-3}. \quad (2.3)$$

Since the electroweak-scale seesaw mechanism that is needed to reproduce neutrino data [49, 50] in the $\mu\nu$ SSM is determined by the neutrino Yukawa couplings $Y_\nu \lesssim 10^{-6}$, this dictates a very small mixing between the photino and the neutrinos giving rise to the approximate range for $|U_{\tilde{\gamma}\nu}|^2$ [10]:

$$10^{-16} \lesssim |U_{\tilde{\gamma}\nu}|^2 \lesssim 10^{-12}. \quad (2.4)$$

Taking into account eq. (2.3), this estimate implies that the gravitino will be very long lived compared to the current age of the Universe, which is about 4×10^{17} s. As discussed in [10], one can carry out the numerical analysis of the whole low-energy parameter space of the $\mu\nu$ SSM, confirming the result (2.4). Nevertheless, these bounds are very conservative, and in fact the results of the numerical scan in [10] favour the much smaller range:

$$10^{-15} \lesssim |U_{\tilde{\gamma}\nu}|^2 \lesssim 5 \times 10^{-14}. \quad (2.5)$$

It is worth noting that in the scan of ref. [10] the mass of the lightest neutralino is typically above 20 GeV, and since $m_{3/2}$ is constrained to be smaller than a few GeV in the $\mu\nu$ SSM, as discussed in the introduction, the gravitino can safely be used as the LSP. The ranges

³The gravitino could also decay into a W^\pm and a charged lepton, into a Z^0 and a neutrino, or into a Higgs boson and a neutrino [44]. However, these decay channels are not kinematically accessible in our case, since the mass of the gravitino in the $\mu\nu$ SSM must be smaller than about 10 GeV in order to fulfil the observational constraints. Also, because of this upper bound on the gravitino mass, three-body decay modes of the gravitino [45–47] are not relevant, and we will not consider them throughout this work.

⁴The flux of monochromatic neutrinos could be in principle observed in neutrino detectors. However, at energies around 1 GeV the signal is expected to be overwhelmed by atmospheric neutrinos and, given the typically bad neutrino energy resolution, also a spectral analysis is not of much help. Moreover, the effective volume of neutrino detectors in the GeV range is too small to expect a sizeable signal event rate. See ref. [48] for a related discussion. Thus we concentrate on γ -ray line searches throughout this work.

for the photino–neutrino mixing found in eqs. (2.4) and (2.5) together with the formula for the gravitino lifetime, eq. (2.3), give a clear prediction for the expected γ -ray line signal from gravitino decays in the $\mu\nu$ SSM that will be tested against the *Fermi*-LAT data in our analysis below.

Let us finally remark that for the gravitino to be a good DM candidate also requires that it can be present in the right amount to explain the relic density inferred by cosmological observations, $\Omega_{\text{DM}} h^2 \simeq 0.1$. We will discuss this issue in the next subsection.

2.2 Gravitino relic density

An inflationary phase in the early Universe, as supported by many cosmological observations, would dilute any primordial abundance of gravitinos. In many cases, depending on the values of the reheating temperature T_R and $m_{3/2}$, the gravitino would not reach thermal equilibrium with the rest of the hot plasma after inflation [51]. Still, gravitinos could be produced in scattering processes in the thermal bath. The relic density of gravitinos from thermal production (TP) in the early Universe is given by [52]:

$$\Omega_{3/2}^{\text{TP}} h^2 \simeq \sum_{i=1}^3 \omega_i g_i^2 \left(1 + \frac{M_i^2}{3 m_{3/2}^2} \right) \ln \left(\frac{k_i}{g_i} \right) \left(\frac{m_{3/2}}{100 \text{ GeV}} \right) \left(\frac{T_R}{10^{10} \text{ GeV}} \right), \quad (2.6)$$

where the sum runs over the SM gauge groups. The numerical factors are given by $\omega_i = (0.018, 0.044, 0.117)$ and $k_i = (1.266, 1.312, 1.271)$. The gauge couplings g_i and the gaugino masses M_i are understood to be evaluated at an energy corresponding to the reheating temperature. The one-loop renormalisation group equations for these parameters are given by [53]:

$$g_i(T_R) = \left[g_i(m_Z)^{-2} - \frac{\beta_i^{\text{SM}}}{8\pi^2} \ln \left(\frac{m_{\text{SUSY}}}{m_Z} \right) - \frac{\beta_i^{\text{SUSY}}}{8\pi^2} \ln \left(\frac{T_R}{m_{\text{SUSY}}} \right) \right]^{-1/2}, \quad (2.7)$$

$$M_i(T_R) = \left(\frac{g_i(T_R)}{g_i(m_Z)} \right)^2 M_i(m_Z), \quad (2.8)$$

where the SM beta function coefficients are $\beta_i^{\text{SM}} = (41/6, -19/6, -7)$, the MSSM beta function coefficients are $\beta_i^{\text{SUSY}} = (11, 1, -3)$ ⁵ and the values for the gauge couplings at the electroweak scale are $g_2(m_Z) \equiv g(m_Z) = m_W \sqrt{8 G_F / \sqrt{2}} \simeq 0.65$, $g_1(m_Z) \equiv g'(m_Z) = g_2(m_Z) \tan \theta_W(m_Z) \simeq 0.36$ and $g_3(m_Z) \equiv g_s(m_Z) = \sqrt{4\pi \alpha_s(m_Z)} \simeq 1.22$ [54]. In these expressions m_W and m_Z are the masses of the W and Z bosons, respectively, and G_F is the Fermi constant. We assume a supersymmetry mass scale $m_{\text{SUSY}} \sim 1 \text{ TeV}$.

Equation (2.6) only holds for gravitino densities well below the thermal equilibrium density since only gravitino production processes and no reverse processes are taken into account in the derivation [52, 55]. That is, in cases where we want to fix the gravitino abundance to the measured DM density in the Universe, the formulae are valid for gravitino masses above $\mathcal{O}(1) \text{ keV}$ [56]. Moreover, the derivation makes use of an expansion in the coupling constants that is only well justified for temperatures $T_R \gg 10^6 \text{ GeV}$ [52, 55]. Thus the extrapolation to lower reheating temperatures may not be entirely reliable, but it is the best estimate we have at this time.

⁵As the $\mu\nu$ SSM only extends the particle content compared to the MSSM by three right-handed neutrinos, the β function coefficients do not change.

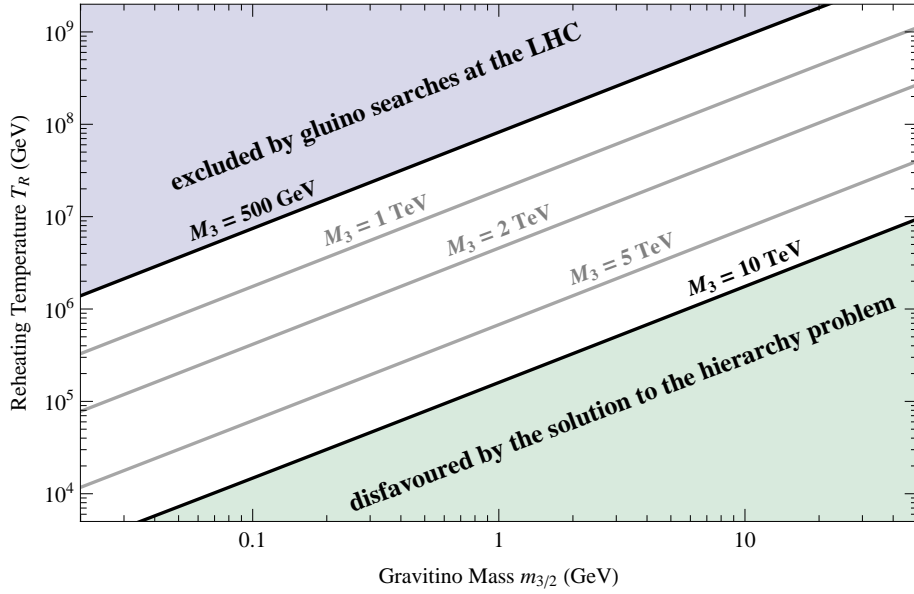


Figure 1. Parameter space for the gravitino DM scenario in the $m_{3/2}$ – T_R plane. The diagonal lines show the contours where the gravitino relic density matches the observed DM density for the indicated value of the gluino mass according to eq. (2.6). We assume universal gaugino masses at the GUT scale. The barely visible widths of the lines correspond to the 3σ uncertainty of the cosmological data. The areas above the $M_3 = 500$ GeV line and below the $M_3 = 10$ TeV line are excluded.

In figure 1 we show the gravitino mass–reheating temperature plane. If we require the gravitino abundance to match the abundance of cold DM in the Universe as determined by a combination of different cosmological observables, $\Omega_{\text{DM}} h^2 = 0.1187 \pm 0.0017$ [2], fixed values for the gaugino masses correspond to lines in this plane. The widths of those lines correspond to the 3σ uncertainty of the cosmological data, thus showing the high level of accuracy in the experimental determination of the DM relic density. We show here the situation for the case of universal gaugino masses at the GUT scale, corresponding to mass ratios of $M_3 \simeq 2.8 M_2 \simeq 5.1 M_1$ at the scale $m_{\text{SUSY}} \sim 1$ TeV. Giving up this relation will change the picture but the results remain similar at least as long as the gluino is the heaviest of the gauginos. The ATLAS and CMS collaborations at the LHC have performed several searches for signals of supersymmetry, so far without success. Depending on the model assumptions they find lower limits on the gluino mass M_3 ranging from several hundred GeV to beyond a TeV [57, 58]. There are currently no gluino mass limits by the LHC collaborations for the specific case of the $\mu\nu\text{SSM}$ or models with gravitino DM and R -parity violation in general. Thus, for definiteness we use in figure 1 a conservative lower limit of 500 GeV. On the other hand, we expect a gluino mass below $\mathcal{O}(10)$ TeV to solve the hierarchy problem by means of supersymmetry. This leaves us with the white area as the viable parameter space for gravitino DM.

As we will discuss below, strong bounds on the parameter space of decaying gravitino DM can be derived from γ -ray line searches. The result of our analysis allows us to limit the gravitino mass to values below 4.8 GeV in the case of the $\mu\nu\text{SSM}$ (see section 4.1).⁶ This result,

⁶Since the mechanism of supersymmetry breaking is unknown, in supergravity models like the $\mu\nu\text{SSM}$ the gravitino mass is basically a free parameter. However, one can apply observational constraints like the lower

in turn, restricts the reheating temperature to be below $\sim 4 \times 10^8 \text{ GeV}$ (cf. figure 1).⁷ As mentioned in the introduction, it has been found that in the context of the $\mu\nu\text{SSM}$ the baryon asymmetry of the Universe can be generated by the mechanism of electroweak baryogenesis which does not require a very high value of the reheating temperature [31]. Other possibilities, like the popular mechanism of thermal leptogenesis [62], are in tension with the upper limit on the reheating temperature found above. However, leptogenesis is disfavoured anyway in the context of the $\mu\nu\text{SSM}$ since the model exhibits an electroweak-scale seesaw mechanism.

Apart from producing the correct relic density, common problems in supergravity theories are conflicts with the predictions of big bang nucleosynthesis (BBN) due to late decays of the next-to-lightest supersymmetric particle (NLSP) into the gravitino [63]. In the $\mu\nu\text{SSM}$ this problem is easily evaded since the NLSP decays well before the onset of BBN via R -parity breaking interactions (see ref. [34] for a related discussion).

Let us conclude this section with the remark that there is plenty of parameter space for a gravitino LSP with the correct relic density and leading to a consistent cosmological scenario fulfilling all current constraints.

3 Search for γ -ray lines from below 10 GeV in the *Fermi*-LAT data

3.1 Gamma-ray flux and dark matter distribution

Cosmological N-body simulations predict the inner part of the Galaxy to enclose the highest DM density and have inspired parametrisations of the DM halo distribution. We calculate the differential flux of γ rays from DM decays in the Galactic halo by integrating one particular DM distribution along the line of sight. We assume here two-body decays producing monochromatic γ rays and neutrinos. In this case the flux reads:

$$\frac{d\Phi_{\gamma, \text{dec}}^{\text{halo}}}{dE} = \frac{1}{4\pi\tau_{\gamma\nu}m_{\text{DM}}} \delta\left(E - \frac{m_{\text{DM}}}{2}\right) \int_{\Delta\Omega} \cos b \, db \, d\ell \int_0^\infty ds \, \rho_{\text{halo}}(r(s, b, \ell)), \quad (3.1)$$

where b and ℓ denote the Galactic latitude and longitude, respectively, and s denotes the distance from the Solar System. Furthermore, m_{DM} and $\tau_{\gamma\nu}$ are the DM mass and lifetime (here inverse decay width for $\text{DM} \rightarrow \gamma\nu$), respectively, $\Delta\Omega$ is the region of interest (ROI), and δ denotes the Dirac delta distribution. The radius r in the DM halo density profile of the Milky Way, ρ_{halo} , is expressed in terms of these Galactic coordinates,

$$r(s, b, \ell) = \sqrt{s^2 + R_\odot^2 - 2sR_\odot \cos b \cos \ell}. \quad (3.2)$$

In this expression $R_\odot \simeq 8.5 \text{ kpc}$ [64–66] is the radius of the solar orbit around the Galactic Centre. The corresponding formula for the γ -ray flux from self-conjugate DM annihilations via $\text{DM DM} \rightarrow \gamma\gamma$ reads:

$$\frac{d\Phi_{\gamma, \text{ann}}^{\text{halo}}}{dE} = \frac{\langle\sigma v\rangle_{\gamma\gamma}}{8\pi m_{\text{DM}}^2} 2\delta(E - m_{\text{DM}}) \int_{\Delta\Omega} \cos b \, db \, d\ell \int_0^\infty ds \, \rho_{\text{halo}}^2(r(s, b, \ell)), \quad (3.3)$$

limit of 1.2 keV on the mass of warm DM particles derived from Lyman-alpha forest data [59, 60].

⁷Since there is no unique theory of inflation and the reheating phase of the early Universe, there are almost no theoretical constraints on the value of the reheating temperature. From observational constraints the reheating temperature could be as low as a few MeV [61].

where $\langle\sigma v\rangle_{\gamma\gamma}$ is the thermal-averaged DM annihilation cross section into two photons. For the later discussion it is useful to define J -factors, which are directly proportional to the relevant line-of-sight integral and the signal flux in a given ROI that spans the solid angle $\Delta\Omega_{\text{ROI}}$,

$$J_{\text{dec (ann)}} = \int_{\Delta\Omega_{\text{ROI}}} \cos b \, db \, d\ell \int_0^\infty ds \, \rho_{\text{halo}}^{1(2)}(r(s, b, \ell)) . \quad (3.4)$$

Throughout this analysis we will employ the Einasto profile with a finite central density [67, 68]:

$$\rho_{\text{Ein}}(r) = \rho_\odot \exp\left(-\frac{2}{\alpha} \left(\left(\frac{r}{r_s}\right)^\alpha - \left(\frac{R_\odot}{r_s}\right)^\alpha\right)\right), \quad (3.5)$$

where we adopt $\alpha = 0.17$ and $r_s = 20 \text{ kpc}$ for the case of the Milky Way and a local DM density of $\rho_\odot \simeq 0.4 \text{ GeV cm}^{-3}$ [66, 69, 70]. In appendix A we consider other DM halo profiles as well as uncertainties on the halo parameters and quantify the impact of the choices on our results.

3.2 Selection and processing of *Fermi*-LAT data

We search for γ -ray spectral lines from 100 MeV to 10 GeV. To include the spectral sidebands for all fit points, we consider data from 56.5 MeV to 11.5 GeV. For our dataset we use the P7REP_CLEAN event selection on data taken between August 4, 2008, and October 15, 2013 by the *Fermi*-LAT. We chose to use the stringent P7REP_CLEAN event selection since it has low residual cosmic-ray contamination compared to the γ -ray flux. More information about the *Fermi*-LAT instrument, performance, and data usage can be found in refs. [11, 71] as well as the FSSC website.⁸ A short overview of the *Fermi*-LAT instrument and event class naming convention can be found in section II of ref. [16].

The version of the instrument response functions (IRFs) that we used in this work is P7REP_CLEAN_V15. We only use events with a measured zenith angle less than 100° to remove the emission from the Earth's limb (i.e. γ rays from cosmic-ray interactions in the upper atmosphere). We also apply the standard good time selection criteria "DATA_QUAL == 1 && LAT_CONFIG == 1 && abs(ROCK_ANGLE) < 52" using the *gtmktime* ScienceTool. Note that the adopted rocking angle cut is only applicable to data taken prior to December 6, 2013, which is the case for our dataset. The initial data reduction and exposure calculations were performed using the *Fermi*-LAT ScienceTools version 09-32-02.⁹ Further details about the data selection cuts in signal and control regions can be found in appendix B.

We have not performed any point source masking and do not include point sources in our fitting procedure. We choose not to mask sources because at the low end of the energy range of our dataset, the 68% containment radius of the *Fermi*-LAT point-spread function (PSF) is $\gtrsim 5^\circ$ [71], which would cause us to mask almost the entire dataset given the large number of known γ -ray point sources. However, γ -ray point sources are not expected to produce narrow line-like spectral features; we will quantify the systematic uncertainties that follow from our analysis choices in section 3.5.

3.3 Region of interest optimisation

Since a DM signal would have a very different morphology from the dominant astrophysical γ -ray emission, optimising the ROIs used is critical for an efficient search for γ -ray lines [17,

⁸The *Fermi*-LAT photon data are available at <http://fermi.gsfc.nasa.gov/ssc/>.

⁹<http://fermi.gsfc.nasa.gov/ssc/data/analysis/software/>

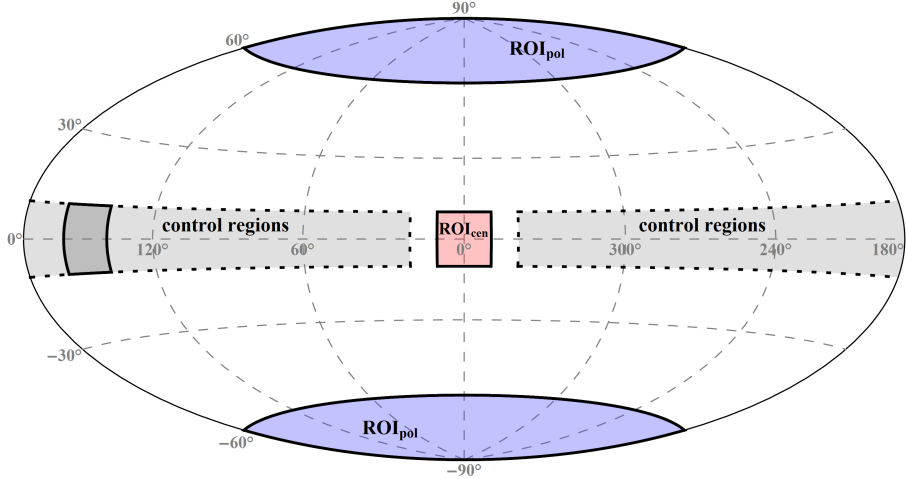


Figure 2. Skymap of ROIs used in this analysis; plotted in Galactic coordinates using the Hammer–Aitoff projection. The region ROI_{pol} (blue) is optimised for the signal-to-background ratio in the case of DM decay, while the region ROI_{cen} (red) is optimised for the signal-to-background ratio in the case of DM annihilation. The dashed line encloses the area for the control regions along the Galactic plane (light grey), while the grey region is an example of one of the 31 control regions used in this analysis.

[72]. In cases where the search is background limited and systematics can be neglected, the statistical power of a line search is maximised if the signal-to-noise ratio, $n_{\text{sig}}/\sqrt{b_{\text{eff}} + n_{\text{sig}}}$, within the ROI is maximal. Here, n_{sig} denotes the number of expected signal events, b_{eff} the number of effective background events (for a definition see Eq. (3.11) below), and a useful common assumption is that $n_{\text{sig}} \ll b_{\text{eff}}$. An optimisation with respect to this signal-to-noise ratio is relevant in searches for γ -ray lines at intermediate and high *Fermi*-LAT energies. However, as we will discuss below in more detail, at energies $\lesssim 3$ GeV the search will be limited by systematic effects that scale approximately linearly with the number of background γ rays. In that case, an optimal ROI should rather maximise the signal-to-background ratio, $n_{\text{sig}}/b_{\text{eff}}$, in order to achieve maximal discrimination power between a real signal, an instrumental effect and background modelling uncertainties.

In the present analysis, we select two ROIs that optimise the signal-to-background ratio for searches for decay and annihilation signals, respectively. The details of the ROI optimisation process are in appendix C. For our analysis, we selected the following two ROIs:

$$\text{ROI}_{\text{pol}}: |b| > 60^\circ \quad \text{for decay, and} \quad (3.6)$$

$$\text{ROI}_{\text{cen}}: (|b| < 10^\circ \text{ and } |\ell| < 10^\circ) \quad \text{for annihilation,} \quad (3.7)$$

where the decay ROI includes the Galactic poles and the annihilation ROI includes the Galactic Centre. Note that the size of the search region ROI_{cen} is chosen in order to be larger than the PSF at low energies (the 68% containment at 100 MeV is $\sim 5^\circ$). The signal-to-background ratio for the ROI_{cen} region is roughly a factor of two less than the optimal value would be if the PSF could be neglected. The positions and sizes of these regions are indicated in figure 2. We calculated the J -factors corresponding to an annihilation or decay signal for both regions. In case of the Einasto profile, they are $J = 2.89 \times 10^{22} \text{ GeV cm}^{-2}$ for decay and $J = 8.89 \times 10^{22} \text{ GeV}^2 \text{ cm}^{-5}$ for annihilation. The J -factors for other DM profiles are given in appendix A.

3.4 Fitting procedure

Our search for a line signal in the *Fermi*-LAT data, as well as the derivation of upper limits on line fluxes, is based on the profile likelihood method (see e.g. ref. [73]). We model the sum of the astrophysical γ -ray background and the cosmic-ray contamination of the P7REP_CLEAN data empirically by a single power law with free normalisation and spectral index. Since the power-law approximation is only valid locally and breaks down when considering large enough energy ranges, we restrict the fit to small energy ranges centred around and moving with the line energy. In the present work, we adopt an energy range of $(E_\gamma - 2\sigma_E, E_\gamma + 2\sigma_E)$, where E_γ denotes the line energy of interest, and σ_E/E_γ is the energy resolution at that energy ($\pm\sigma_E$ is the 68% containment range). We selected this energy range as a compromise between a loss of statistical power in smaller ranges, and increasing systematic uncertainties in cases of larger ranges. Each fit was performed at a fixed energy, E_γ , in steps of $0.5\sigma_E$, where σ_E ranges from 20% of E_γ at 100 MeV to 10% of E_γ at 10 GeV. We used the RooFit toolkit [74] (version 3.12) to implement the models and perform the likelihood minimisation.

At the low energies of interest, the number of photon events in our analysis is very large. For computational efficiency, we perform a binned maximum likelihood fit to the data, with a bin width of $0.066\sigma_E$ (i.e. 60 bins over the $\pm 2\sigma_E$ energy window). Furthermore, we take into account the possibility that the true number of signal events, n_{sig} , is systematically offset by n_{syst} from the best fit value, n'_{sig} . In other words, we only consider the true signal events to be those that remain after subtracting the expected systematic offset, $n_{\text{sig}} = n'_{\text{sig}} - n_{\text{syst}}$, and taking into account its variance. The full likelihood function that we adopt in our analysis is based on the product of the Poisson likelihoods (P) to observe c_i counts in each energy bin:

$$\mathcal{L}(\alpha, \Gamma, n_{\text{sig}}, n_{\text{syst}}) = P_{\mathcal{F}}(n_{\text{syst}}, b_{\text{eff}}) \prod_i P(c_i | \mu_i(\alpha, \Gamma, n_{\text{sig}} + n_{\text{syst}})) , \quad (3.8)$$

where the expected number of events in the i -th energy bin ($E_i^- \equiv E_\gamma - 2\sigma_E, E_i^+ \equiv E_\gamma + 2\sigma_E$) is given by

$$\mu_i(\alpha, \Gamma, n'_{\text{sig}}) = \int_{E_i^-}^{E_i^+} dE (\alpha E^{-\Gamma} \mathcal{E}(E) + n'_{\text{sig}} \cdot \mathcal{D}_{\text{eff}}(E|E_\gamma)) , \quad (3.9)$$

and $\mathcal{D}_{\text{eff}}(E|E_\gamma)$ denotes the energy dispersion of the *Fermi*-LAT. Furthermore, $\mathcal{E}(E)$ denotes the energy-dependent exposure of the ROI, Γ and α are the spectral index and normalisation of the power-law background, b_{eff} is the effective number of background events in the energy range covered by the line signal, n_{syst} is the additive systematic error (to be discussed below), and $P_{\mathcal{F}}$ is the distribution of n_{syst} , which we model to be independent of energy. Note that we actually fitted for $n_{\text{bkg}} = \int \alpha E^{-\Gamma} \mathcal{E}(E) dE$, the total number of events in the power-law background, rather than α directly.

As discussed in appendix C5 of ref. [16], \mathcal{D}_{eff} varies slightly depending on the “observing profile” (i.e. the amount of observing time for each event incident angle, θ). To account for this in our search, we modelled \mathcal{D}_{eff} for each fit similar to what was done in ref. [17]. Specifically, we integrated the energy- and θ -dependent representation of the energy dispersion provided with the *Fermi*-LAT IRFs over the observing profile for the regions of interest and then fit a triple Gaussian (sum of three Gaussian functions) parametrisation to that shape to serve as our \mathcal{D}_{eff} model.

We furthermore investigated the effect of including additional information in our \mathcal{D}_{eff} model that quantified the quality of the energy reconstruction on an event-by-event basis,

since it is expected to improve the statistical power of the search (see section IV of ref. [16]). We found that while this improvement was important in searches for higher-energy spectral lines ($\sim 15\%$ increase in statistical power for $E \gtrsim 10$ GeV), it was less than 10% at lower energies, and is hence neglected in the present analysis. At higher energies the quality of the energy reconstruction can vary markedly from event to event. For example, an on-axis 100 GeV γ -ray event leaks about 50% of its energy out the back of the *Fermi*-LAT [71]. Events at this energy with larger incident angles will travel through more radiation lengths in the *Fermi*-LAT calorimeter, leak less energy out the back, and therefore typically have more accurate energy reconstructions. However, the difference between the quality of the energy reconstruction is less dramatic at lower energies ($\lesssim 1$ GeV), where the energy deposition is usually fully contained in the *Fermi*-LAT calorimeter.

The most relevant effect of any systematic biases that masks or fakes a line-like signal (this includes both instrumental effects as well as effects due to the power-law approximation of the background spectra) is to offset the estimated number of signal events with respect to its true value. We expect such offsets to scale linearly with the number of events in the ROI; therefore it is useful to introduce the *fractional deviation* f , which, roughly speaking, denotes the fractional size of a line signal relative to the background under the signal peak (similar to signal-to-background ratio):

$$f \equiv n_{\text{sig}}/b_{\text{eff}}, \quad (3.10)$$

where b_{eff} denotes the number of effective background events below a line signal. For each ROI and value of E_γ , the number of effective background events is obtained as

$$b_{\text{eff}} = \int_{E_i^-}^{E_i^+} dE \frac{\mathcal{D}_{\text{eff}}(E|E_\gamma) \alpha E^{-\Gamma} \mathcal{E}(E)}{\alpha E^{-\Gamma} \mathcal{E}(E) + \mathcal{D}_{\text{eff}}(E|E_\gamma)}, \quad (3.11)$$

where α and γ are determined from a power-law only fit to the data (with $n'_{\text{sig}} = 0$ fixed).

A systematic uncertainty in the number of signal events can now be conveniently expressed as being proportional to the fractional deviation, δf . For most systematically induced features that could fake or hide a line signal, this quantity will be approximately independent of the number of measured events in the adopted ROI. The corresponding distribution function, $P_{\mathcal{F}}(n_{\text{syst}}, b_{\text{eff}})$ in eq. (3.8), will be determined empirically as discussed in the next subsection.

As usual, upper limits at the 95% confidence level (CL) on the number of signal events n_{sig} are obtained by increasing n_{sig} , while refitting all other parameters, until $-2 \ln \mathcal{L}$ changes by 2.71 from its best-fit value. The significance of a line signal in units of Gaussian sigma is given by $\sqrt{2 \ln \mathcal{L} / \mathcal{L}_0}$, where \mathcal{L}_0 denotes the likelihood of a fit with the line flux set to zero. Note that in our analysis, we neglect corrections to the finite angular resolution of the *Fermi*-LAT. Furthermore, by construction, effects related to modelling uncertainties (i.e. modelling the effective area, background emission, and not masking known point sources) are absorbed in $P_{\mathcal{F}}(n_{\text{syst}}, b_{\text{eff}})$.

3.5 Systematics

As discussed in section VI of ref. [16], there are three classes of systematic uncertainties involved when searching for γ -ray spectral lines: uncertainties on the calculated exposure ($\delta \mathcal{E} / \mathcal{E}$), uncertainties on the fit estimates of the signal counts ($\delta n_{\text{sig}} / n_{\text{sig}}$), and line-like uncertainties that could mask a true signal or induce a false signal (δf) that we discussed in

the previous subsection. The two former are less worrisome since they are smaller than the statistical uncertainty on the 95% CL limit on n_{sig} ($\sim 50\%$ since $n_{\text{sig}} \ll b_{\text{eff}}$, causing the statistical uncertainty on n_{sig} to be $\simeq \sqrt{b_{\text{eff}}}$), and can safely be neglected.

The latter systematic uncertainties are especially worrisome since positive features could induce false signals, while negative features could mask true signals. We quantify these in terms of an uncertainty on the fractional deviation (see eq. (3.10)), δf . The statistical uncertainty is $\delta f_{\text{stat}} \simeq 1/\sqrt{b_{\text{eff}}}$, while systematically induced fractional deviations are expected to be $\delta f_{\text{syst}} \simeq \text{constant}$. Therefore, as b_{eff} increases (i.e. the number of events used in the fit increases), the systematic uncertainties can begin to dominate ($\delta f_{\text{stat}} \ll \delta f_{\text{syst}}$). This is the case for all of our low energy fits ($E_\gamma \lesssim 3 \text{ GeV}$), which is why it is necessary to include systematic uncertainties correctly in the fitting procedure.

As mentioned in the previous subsection, we incorporate the systematic uncertainties into our likelihood formalism via $P_{\mathcal{F}}(n_{\text{syst}}, b_{\text{eff}})$ (see eq. (3.8)). We break the degeneracy between n_{syst} and n_{sig} by constraining n_{syst} with a Gaussian distribution¹⁰

$$P_{\mathcal{F}}(n_{\text{syst}}, b_{\text{eff}}) = \frac{1}{\sigma_{\text{syst}} \sqrt{2\pi}} \exp \left(-\frac{(n_{\text{syst}} - \mu_{\text{syst}})^2}{2\sigma_{\text{syst}}^2} \right). \quad (3.12)$$

We chose to set $\mu_{\text{syst}} = 0$ and define $\sigma_{\text{syst}} = \delta f_{\text{syst}} b_{\text{eff}}$, where δf_{syst} was determined based on fits for line-like signals in control regions. One could model n_{syst} more aggressively, for example in an energy-dependent way, but we chose not to since we have only a limited number of control regions available to verify the energy dependence of n_{syst} .

We fit for line-like signals in control regions where we do not expect any DM signal to dominate in order to estimate δf_{syst} . We scan in $0.25\sigma_E$ steps in energy for line-like signals (allowing for both positive and negative signals) in $20^\circ \times 20^\circ$ ROIs along the Galactic plane in 10° steps excluding the 5 centre-most ROIs (i.e. $|b| > 20^\circ$; 31 total ROIs; cf. figure 2). Since the DM signal is expected to peak in the Galactic Centre, this is a control region where non-DM astrophysical processes dominate the observed γ -ray emission. Systematically induced line-like features will result from modelling imperfections like averaging the energy-dependent variations in the *Fermi*-LAT effective area over the ROI, not masking or modelling known point sources, and modelling the background spectrum as a power law. It is not possible to disentangle these components in our Galactic plane scans, so we consider them together as modelling imperfections. We also studied the fractional deviations observed in γ rays from the Earth's limb emission and the Vela pulsar, see appendix B.

Figure 3 shows the fractional deviations observed in the Galactic plane scan. Also shown is the average statistical uncertainty of the fractional deviation. If there were no systematic effects, one would expect δf_{stat} to contain 68% of the observed fractional deviations. Clearly this is not the case, especially at lower energies, showing that systematic effects are not negligible. At high energies, $\gtrsim 3 \text{ GeV}$, the fits are dominated by statistical variations, while at lower energies the fits are dominated by systematic effects. We calculated the δf values that contained 68% of the Galactic plane fits, $\delta f_{68}(E)$, in a small energy range ($\pm 10\%$). To be conservative, we choose the largest δf_{68} value observed in the Galactic plane scan (for $E_\gamma < 3 \text{ GeV}$) as our estimate for the systematic uncertainty from biases in our modelling of the LAT effective area, point-source contributions, and the background spectral shape; $\delta f_{\text{GP}} = 0.011$.

¹⁰We also studied modeling n_{syst} with top hat and triangle functions with a base width of $2\delta f_{\text{stat}}$. They improved and worsened the limits by $\sim 30\%$ respectively. Given our choice of $\delta f_{\text{stat}} = 0.011$, we consider this modeling choice to be simple, but conservative.

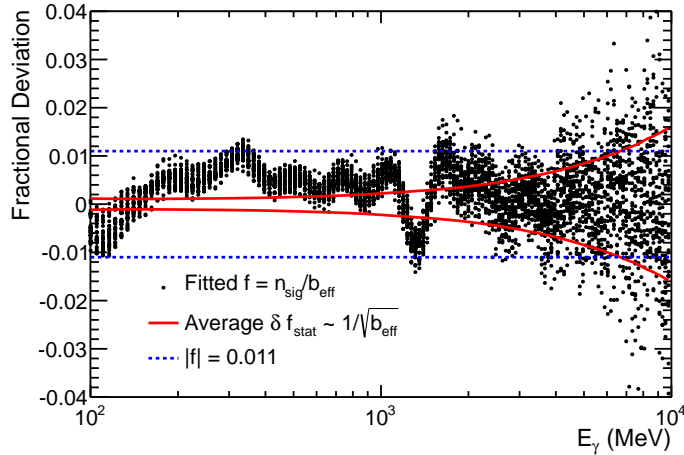


Figure 3. Fractional deviations (f , see eq. (3.10)) observed in the Galactic plane scan are shown as black dots. E_γ went from 100 MeV to 10 GeV in steps of $0.25\sigma_E$. The red line shows the average statistical uncertainty from the Galactic plane scan. The blue dashed line shows the value we chose to represent the δf from modelling biases; see text for details.

From figure 3, we can infer some properties of the systematic uncertainties that affect our search. The displacement of δf from zero and common variations with energy between all the control ROIs are most likely caused by small biases in modelling the *Fermi*-LAT effective area. The spread amongst the fits in the control ROIs is probably from our modelling of the background spectra by a power law.

We also estimate the systematic uncertainty from residual cosmic-ray events passing our γ -ray event selection. Since we use the P7REP_CLEAN event class, the cosmic-ray contamination is not expected to be a large effect, especially for the region ROI_{cen}, which focuses on the bright Galactic Centre. However, cosmic-ray contamination is worrisome at large latitudes (e.g. ROI_{pol} region). To study the effect of cosmic-ray contamination, we select events that are included in the less stringent P7REP_SOURCE class, but are not included in the P7REP_CLEAN class in the ROI_{pol} region. This sample will be enriched with cosmic-ray events that were not removed by the P7REP_SOURCE selection, but did not pass the P7REP_CLEAN event selection. Similar to what was done in ref. [16], we take the largest observed δf in this control sample along with the expected γ -ray acceptance ratio between the P7REP_CLEAN and P7REP_SOURCE selections (see appendix D5 in ref. [16]) to obtain an estimate of $\delta f_{\text{CR}} \sim 0.001$ and $\delta f_{\text{CR}} \sim 0.01$ in ROI_{cen} and ROI_{pol} respectively. Therefore we obtain a final estimate of $\delta f_{\text{syst}} = 0.011$ and $\delta f_{\text{syst}} = 0.015$ in ROI_{cen} and ROI_{pol} respectively.

Other systematic uncertainties in this search enter from our calculation of the *Fermi*-LAT exposure, modelling of the energy dispersion, and our choice of E_γ grid spacing. The overall uncertainty in the calculation of the *Fermi*-LAT effective area is $\sim 10\%$. Additionally, we choose to use the average exposure across our ROIs when converting from counts to flux. The *Fermi*-LAT observes the sky with relative uniform exposure, but it does vary by $\delta\mathcal{E}/\mathcal{E} = 0.02$ in ROI_{cen} and by $\delta\mathcal{E}/\mathcal{E} = 0.07$ in ROI_{pol}. When added in quadrature, we have a total systematic uncertainty on the exposure of $\delta\mathcal{E}/\mathcal{E} = 0.10$ and $\delta\mathcal{E}/\mathcal{E} = 0.12$ in ROI_{cen} and ROI_{pol} respectively. Additionally, we estimate the effect of the 10% uncertainty in the energy resolution [71] to be $\delta n_{\text{sig}}/n_{\text{sig}} \simeq 7\%$. Also, fitting at fixed E_γ values with a grid spacing of $0.5\sigma_E$ would cause us to undermeasure the number of signal counts by 10% at

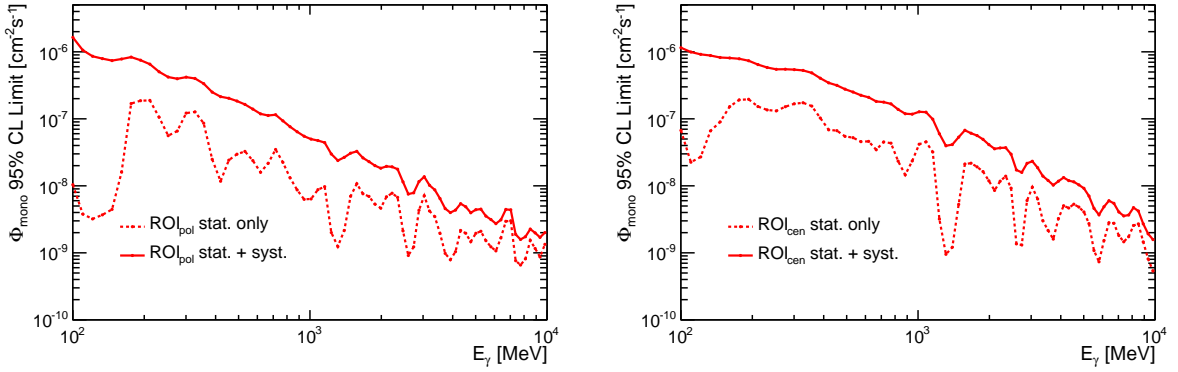


Figure 4. 95% CL Φ_{mono} upper limits in ROI_{pol} (left) and ROI_{cen} (right). The solid line shows the limits obtained using δf_{syst} values determined from fits in our control regions. The dashed line shows the limits obtained neglecting the systematic uncertainties ($\delta f_{\text{syst}} = 0$).

most if the true line were in between two fit points. Therefore, the total uncertainty on the number of signal counts is $\delta n_{\text{sig}}/n_{\text{sig}} = {}^{+0.07}_{-0.12}$. These systematic uncertainties, however, would simply scale our limits up or down by the reported uncertainties, which are smaller than the expected statistical variation of the limits ($\sim 50\%$), and hence neglected.

3.6 Results

We scanned for γ -ray lines from 100 MeV to 10 GeV in both ROI_{cen} (annihilation-optimised) and ROI_{pol} (decay-optimised) and find no significant detections. Note that all our fits had signals with a significance less than 1σ , which is likely an indication that our assignment of δf_{syst} is rather conservative. As discussed above, independent verification of both the magnitude and energy dependence of δf_{syst} is not available. Therefore we chose to simply treat δf_{syst} as a constant determined by fits in our control regions (see section 3.5).

We set 95% CL upper limits on n_{sig} using the method described at the end of section 3.4 at each energy in both ROIs. For a monochromatic signal we can convert the n_{sig} upper limits to flux upper limits using the ROI-averaged exposure $\mathcal{E}_{\text{ROI}}(E_\gamma)$:

$$\Phi_{\text{mono}}(E_\gamma) = \frac{n_{\text{sig}}(E_\gamma)}{\mathcal{E}_{\text{ROI}}(E_\gamma)}. \quad (3.13)$$

Figure 4 shows the 95% CL Φ_{mono} upper limits obtained in ROI_{pol} and ROI_{cen}. We show both the limits obtained assuming no systematic uncertainties ($\delta f_{\text{syst}} = 0$) and those obtained including the appropriate δf_{syst} determined by fits in our control regions.

Assuming the monochromatic signal is coming completely from either DM decay or annihilation, we can find the 95% CL lower limits for $\tau_{\gamma\nu}$ (see eq. (3.1)) and upper limits for $\langle\sigma v\rangle_{\gamma\gamma}$ (see eq. (3.3)), respectively. These limits are shown in figure 5. Furthermore, we provide in appendix D tables of the flux upper limits, the lifetime lower limits and the annihilation cross section upper limits.

4 Discussion

4.1 Implications for $\mu\nu$ SSM gravitino dark matter

Let us finally apply the results obtained above to the case of gravitino DM in the framework of the $\mu\nu$ SSM, assuming that the gravitino constitutes 100% of the DM in the Universe. In

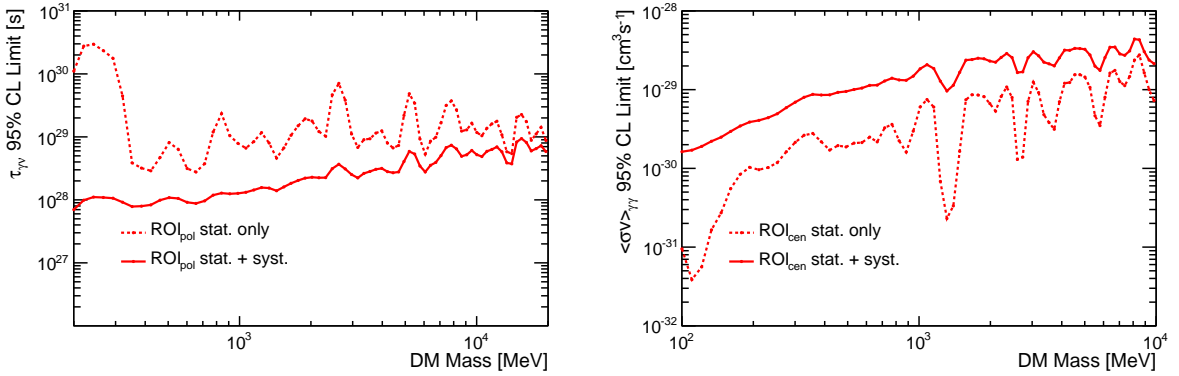


Figure 5. 95% CL $\text{DM} \rightarrow \gamma\nu$ decay lifetime ($\tau_{\gamma\nu}$) lower limits (left) and $\text{DM} \text{DM} \rightarrow \gamma\gamma$ cross section ($\langle\sigma v\rangle_{\gamma\gamma}$) upper limits (right). The solid line shows the limits obtained using δf_{syst} values determined from fits in our control regions. The dashed line shows the limits obtained neglecting the systematic uncertainties ($\delta f_{\text{syst}} = 0$).

figure 6 we show the parameter space for decaying gravitino DM in terms of $\tau_{3/2}$ and $m_{3/2}$ (see figure 7 for the corresponding plot for annihilation signals). The $\mu\nu\text{SSM}$ prediction for the parameter range is shown as a diagonal band bounded by solid lines (see eq. (2.3)). As discussed in section 2, the photino–neutrino mixing parameter is constrained to be in the range shown in eq. (2.4) in order to reproduce the neutrino masses correctly. As a consequence, any acceptable set of gravitino parameters must lie within the diagonal solid lines. The favoured range for the photino–neutrino mixing parameter, eq. (2.5), is coloured in grey in the figure.

The stat. + syst. limit (red thick solid line of figure 6) excludes at 95% CL values of $m_{3/2}$ in the $\mu\nu\text{SSM}$ larger than 4.8 GeV and restricts $\tau_{3/2}$ to be larger than at least 7.9×10^{27} s for lower gravitino masses within the mass range probed by our analysis. Considering the favoured range (grey band), this 95% CL limit implies $m_{3/2}$ to be below 2.4 GeV and $\tau_{3/2}$ to be larger than at least 1.3×10^{28} s for lower gravitino masses. It is worth noting that the stat. + syst. limit is the most robust current bound since we are considering the most relevant systematic effects that may enhance and/or fake a gravitino decay signal. Furthermore, the uncertainty in the DM distribution within the ROI_{pol} target region is rather small (less than $\sim 10\%$) within the context of the local DM density and various DM profiles we consider.

The above results also allow us to discard at 95% CL a large fraction of the $\mu\nu\text{SSM}$ parameter space ($m_{3/2}$, $\tau_{3/2}$) presented in [42], where a gravitino signal was predicted to be detectable through observations of the Virgo galaxy cluster after 5 years of *Fermi*-LAT operation.

4.2 Comparison with previous limits and results

Limits on γ -ray line emission in the energy range 100 MeV to 10 GeV were in the past derived by a number of groups, both for the case of DM decay and for DM annihilation. For comparison, the limits from EGRET observations of the Galactic Centre [43]¹¹, limits using *Fermi*-LAT measurements in a number of ROIs separately optimised for DM decay and DM

¹¹We adopted the limits on the γ -ray flux from the dashed line in figure 7 of ref. [43] (sliding window technique) and calculated the constraints on the lifetime and the annihilation cross section for the case of the Einasto profile adopted in this work. For the $10^\circ \times 10^\circ$ ROI around the Galactic Centre with size $\Delta\Omega_{\text{ROI}} = 0.0304$ sr used in the EGRET analysis, the J -factors are given by $0.522 \times 10^{22} \text{ GeV cm}^{-2}$ for decay and $5.33 \times 10^{22} \text{ GeV}^2 \text{ cm}^{-5}$ for annihilation, respectively.

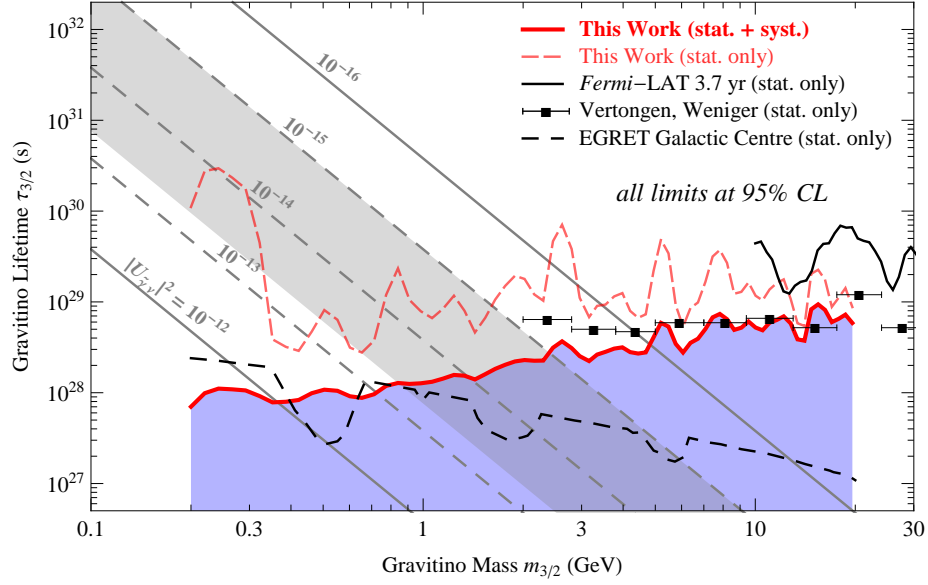


Figure 6. Parameter space of decaying gravitino DM given in terms of the gravitino lifetime and the gravitino mass. The diagonal band shows the allowed parameter space for gravitino DM in the $\mu\nu$ SSM. The numbers on the solid and dashed lines show the corresponding value of the photino–neutrino mixing parameter, as discussed in section 2. The theoretically most favoured region is coloured in grey. We also show several 95% CL lower limits on the gravitino lifetime coming from γ -ray observations. The blue shaded region is excluded by the limits derived in this work.

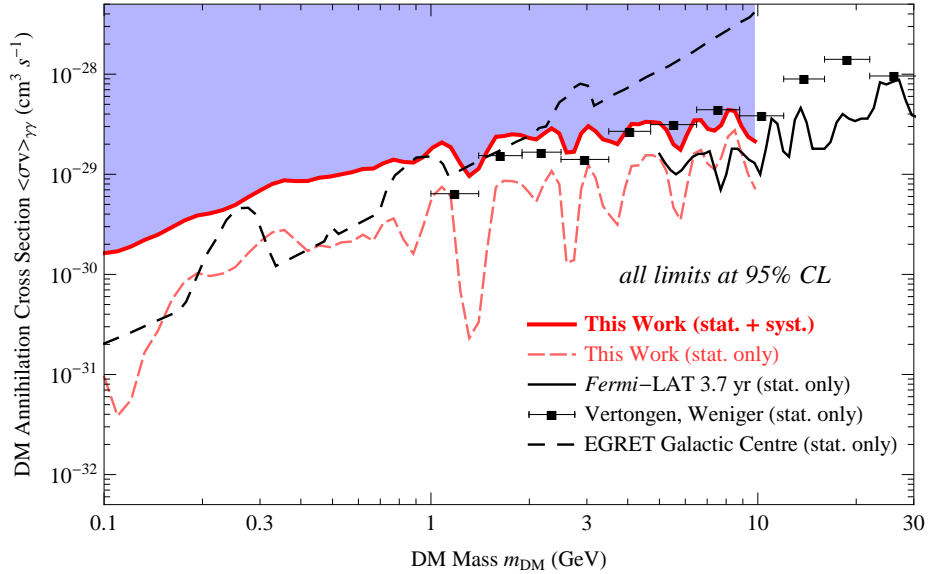


Figure 7. Comparison of the 95% CL upper limits on the DM pair annihilation cross section into two photons found in this work to earlier results using *Fermi*-LAT and EGRET data. The blue shaded region is excluded by the limits derived in this work.

annihilation [16],¹² and limits derived from *Fermi*-LAT data in individual energy ranges [14]¹³

¹²The limits are taken from tables VIII to X of ref. [16]. The cross section limits are those from the ROI R16 optimised for the Einasto profile and the lifetime limits are those from the ROI R180 rescaled by a factor

are also shown in figures 6 and 7. Care has to be taken when comparing these older results with ours, since our limits take systematic effects into account for the first time, whereas all previous analyses were based on statistical errors only. As a consequence, our final limits are — where they overlap — a factor 2–11 (decay) or 2–4 (annihilation) weaker than the limits derived in the high-energy line analysis in ref. [16], and up to a factor of 3 weaker (decay and annihilation) than the conservative limits from ref. [14]. At energies below roughly 400 MeV (decay) or below roughly 1 GeV (annihilation), our limits are furthermore slightly weaker than previous results from EGRET.¹⁴ For comparison we show in figures 6 and 7 the results that we obtain when setting the fractional deviation systematics to zero. In that case, our limits become — as expected for the large effective area of the *Fermi*-LAT — nominally stronger by up to an order of magnitude, and they are in particular stronger than most previous results.

5 Conclusions

In this work we searched for γ -ray lines from 100 MeV to 10 GeV using 5.2 years of *Fermi*-LAT data. We expect these low-energy spectral lines from decaying gravitino DM, but also extend our search to including DM annihilations into a pair of γ rays. We did not find any statistically significant spectral lines and have set robust limits on DM interactions that would produce monochromatic γ rays.

Given the large number of events in our fits, most were dominated by systematic uncertainties since the statistical uncertainties became very small. Therefore, it was critical to appropriately include the systematic uncertainties in our likelihood formalism. For the first time, we present robust limits for monochromatic γ rays that incorporate systematic uncertainties. We conservatively determine the level of systematic uncertainties from fits to control regions where no line-like signals are expected. While our limits are not much more constraining than previous limits, they are more robust.

We discussed the results in the context of the $\mu\nu$ SSM, a Supersymmetric Standard Model that simultaneously solves the μ problem and explains neutrino masses and mixing angles by the addition of right-handed neutrinos to the theory. The gravitino is a well-motivated candidate for the DM as it can have the correct relic density (cf. figure 1) and leads to a consistent cosmological scenario. As a consequence of the γ -ray line search results, the gravitino DM mass in the $\mu\nu$ SSM must be $m_{3/2} < 4.8$ GeV and the lifetime $\tau_{3/2} > 7.9 \times 10^{27}$ s, at 95% CL if we assume that all of the DM in the Universe is in the form of gravitinos. In the favoured model parameter space these limits tighten to $m_{3/2} < 2.4$ GeV and $\tau_{3/2} > 1.3 \times 10^{28}$ s (see figure 6).

Acknowledgments

The *Fermi*-LAT Collaboration acknowledges generous ongoing support from a number of agencies and institutes that have supported both the development and the operation of the *Fermi*-LAT as well as scientific data analysis. These include the National Aeronautics and Space Administration and the Department of Energy in the United States, the Commissariat

2.49/2.46 = 1.01 to account for the J -factor of the Einasto profile as given in table II of ref. [16].

¹³The limits were taken from table 3 of ref. [16] and rescaled with the appropriate factor for the Einasto profile as given in table 2 of ref. [16].

¹⁴The ROI used in the EGRET analysis was considerably smaller than ROI_{cen} . However, recall that we chose to use a $20^\circ \times 20^\circ$ ROI in order to avoid effects from the LAT PSF though the optimal ROI was smaller.

à l’Energie Atomique et aux Energies Alternatives and the Centre National de la Recherche Scientifique / Institut National de Physique Nucléaire et de Physique des Particules in France, the Agenzia Spaziale Italiana and the Istituto Nazionale di Fisica Nucleare in Italy, the Ministry of Education, Culture, Sports, Science and Technology (MEXT), High Energy Accelerator Research Organization (KEK) and Japan Aerospace Exploration Agency (JAXA) in Japan, and the K. A. Wallenberg Foundation, the Swedish Research Council and the Swedish National Space Board in Sweden.

Additional support for science analysis during the operations phase is gratefully acknowledged from the Istituto Nazionale di Astrofisica in Italy and the Centre National d’Études Spatiales in France.

We thank Luca Baldini, Philippe Bruel, Seth Digel, Michael Gustafsson, Daniel E. López-Fogliani, and Miguel Á. Sánchez-Conde for useful discussions and comments.

The work of GAGV was supported by Conicyt Anillo grant ACT1102. GAGV and CM thank for the support of the Spanish MINECO’s Consolider-Ingenio 2010 Programme under grant MultiDark CSD2009-00064. Their work was also supported in part by MINECO under grant FPA2012-34694. GAGV, MG and CM acknowledge the support of the Marie Curie ITN “UNILHC” under grant number PITN-GA-2009-237920, the support by the Comunidad de Madrid under grant HEPHACOS S2009/ESP-1473, and the support of the MINECO under the “Centro de Excelencia Severo Ochoa” Programme SEV-2012-0249. MG also thanks for the support of the Forschungs- und Wissenschaftsstiftung Hamburg through the program “Astroparticle Physics with Multiple Messengers” and the Marie Curie ITN “INVISIBLES” under grant number PITN-GA-2011-289442.

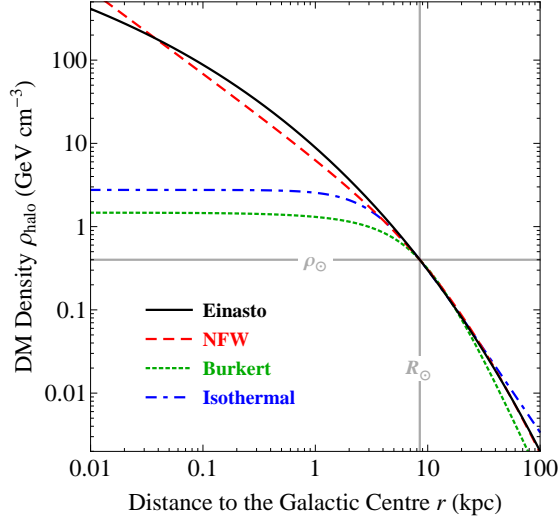


Figure 8. Comparison of different DM density profiles for the Galactic halo.

A Choice of the dark matter halo profile

The distribution of the DM in the Milky Way is not known and therefore presents a source of uncertainty to any analysis of γ -ray signals from DM decay or annihilation. N-body cosmological simulations favour cuspy profiles like the Einasto profile introduced in the main text or the NFW profile [75]:

$$\rho_{\text{NFW}}(r) = \rho_{\odot} \frac{(R_{\odot}/r_s) (1 + R_{\odot}/r_s)^2}{(r/r_s) (1 + r/r_s)^2}, \quad (\text{A.1})$$

where $r_s \simeq 20$ kpc for the case of the Milky Way. By contrast some observations at other halo mass scales favour cored profiles like the isothermal profile [76]:

$$\rho_{\text{iso}}(r) = \rho_{\odot} \frac{1 + (R_{\odot}/r_s)^2}{1 + (r/r_s)^2}, \quad (\text{A.2})$$

where $r_s \simeq 3.5$ kpc for the case of the Milky Way halo [4], or the Burkert profile [77]:

$$\rho_{\text{Bur}}(r) = \rho_{\odot} \frac{(1 + (R_{\odot}/r_s)) (1 + (R_{\odot}/r_s)^2)}{(1 + (r/r_s)) (1 + (r/r_s)^2)}, \quad (\text{A.3})$$

where $r_s \simeq 9$ kpc [78]. In figure 8 we compare the different DM density profiles. In all cases we fixed the normalisation to a local DM density of $\rho_{\odot} \simeq 0.4 \text{ GeV cm}^{-3}$ [66, 69, 70], keeping in mind that this value is rather uncertain and the true value could be up to a factor of 2 lower or higher (see for instance ref. [79] and references therein). Moreover, the value that best fits observational data may depend on the choice of the DM density profile [80, 81]. While all these profiles behave similarly in the outer part of the Milky Way, they deviate significantly in the vicinity of the Galactic Centre. The J -factors that we obtain for the different profiles in our ROIs are summarised in table 1. While the choice of the halo model only introduces an

Profile	ROI	Decay		ROI	Annihilation	
		$\Delta\Omega_{\text{ROI}}$	$J\text{-factor}$		$\Delta\Omega_{\text{ROI}}$	$J\text{-factor}$
		sr	$(10^{22} \text{ GeV cm}^{-2}) \times \left(\frac{\rho_{\odot}}{0.4 \text{ GeV cm}^{-3}}\right)$		sr	$(10^{22} \text{ GeV}^2 \text{ cm}^{-5}) \times \left(\frac{\rho_{\odot}}{0.4 \text{ GeV cm}^{-3}}\right)^2$
Einasto	ROI _{pol}	1.68	2.89	ROI _{cen}	0.121	8.89
NFW	ROI _{pol}	1.68	2.96	ROI _{cen}	0.121	4.81
Isothermal	ROI _{pol}	1.68	3.09	ROI _{cen}	0.121	1.32
Burkert	ROI _{pol}	1.68	2.75	ROI _{cen}	0.121	0.50

Table 1. Summary of the J -factors obtained in the two search regions, for different DM profiles. Our main results assume the Einasto profile and a local DM density $\rho_{\odot} = 0.4 \text{ GeV cm}^{-3}$, but a rescaling to other profiles and other values of ρ_{\odot} is straightforward.

uncertainty on the J -factor of the order of 10% in the case of DM decay, for DM annihilations the J -factors vary by more than an order of magnitude. In addition, the lack of a precise knowledge of parameters like R_{\odot} , α or r_s introduces a sizeable uncertainty on the J -factor even for individual halo profiles. For DM decay this uncertainty is similar in size to the uncertainty introduced by the choice of the halo model. For DM annihilation this uncertainty is also significant, but less important than the choice between a cuspy or a cored halo profile. In addition, the uncertainty on the local DM density enters linearly (decay) or quadratically (annihilation) in the calculation of the J -factors as detailed in table 1. For definiteness we adopted the Einasto profile with $\rho_{\odot} \simeq 0.4 \text{ GeV cm}^{-3}$ as our baseline model when optimising our ROIs and presenting the main results of this paper, but rescaling the results for other profiles and other values of ρ_{\odot} using the values given in table 1 is straightforward.¹⁵

B Other control samples

To further test the effects of uncertainties of the effective area and the background modelling we used two additional control samples along with the Galactic plane scans described in section 3.5: the Earth’s limb and the Vela pulsar. Similarly to the Galactic plane scan, these fits were performed in $0.25\sigma_E$ energy steps. Both samples were used extensively in the validation of the *Fermi*-LAT IRFs [71], and the Earth’s limb has been used as a control sample in previous line searches [15, 16, 82]. These two samples complement each other well; the pulsed emission from Vela cuts off above a few GeV, while the effects of the Earth’s geomagnetic cut-off on cosmic rays significantly complicates modelling the γ -ray emission from the Earth’s limb below a few GeV.

Table 2 shows the data selections for the primary data and the control samples. With the exception of the differences listed in table 2, the initial data preparation for the control

¹⁵Note that while the optimal ROI for the case of DM decay is practically independent of the DM density profile, for the case of DM annihilation the optimal ROI has a fairly strong dependence on the choice of the halo model. Therefore, although the entries in table 1 allow rescaling the limits to other halo models, these limits are not necessarily optimal since the ROIs adopted in our analysis are optimised for an Einasto profile.

¹⁶*Fermi* Mission Elapsed Time is defined as seconds since 2001 January 1, 00:00:00 UTC.

¹⁷For the Vela pulsar sample we require that the entire 22° radius ROI pass the zenith angle selection using the *gtmktime ScienceTool*. This effectively requires $\theta_z < 78^\circ$ at the centre of the ROI.

¹⁸Applied by selecting on `ROCK_ANGLE` with the *gtmktime ScienceTool*.

¹⁹Standard data quality selection: `DATA_QUAL == 1 && LAT_CONFIG == 1` with the *gtmktime ScienceTool*.

Selection	Primary data	Vela pulsar data	Limb data
Observation Period End	2013 Oct. 15	2013 Aug. 8	2013 Jan. 11
Mission Elapsed Time (s) ¹⁶	403509400	379556800	397631400
Fit Energy range (GeV)		0.1–10	3.5–10
ROI	see section 3.3 22° around Vela		-
Zenith range (deg)		$\theta_z < 100$ ¹⁷	$111 < \theta_z < 113$
Rocking angle range (deg) ¹⁸		$ \theta_r < 52$	$ \theta_r > 52$
Data quality cut ¹⁹		yes	yes

Table 2. Summary table of data selections. The observation period for all of the samples began 2008 August 4.

samples were identical to those used from the primary data. For the Vela pulsar control sample we then used the *TEMPO2* package²⁰ [83] and a pulsar timing model²¹ derived from data taken with the Parkes radio telescope [84, 85] to assign a phase with respect to the 89 ms pulse period to each γ ray.

For the Vela pulsar control sample, we fit for a line using only the on-pulse data (γ rays with phases in the ranges $[0.1, 0.3] \cup [0.5, 0.6]$), and used the off-pulse data (γ rays with phases in the range $[0.7, 1.0]$) as a spectral model for the astrophysical emission in the ROI not associated with the Vela pulsar. We then modelled on-pulse flux of the Vela pulsar emission using a power law with a hyper-exponential cut-off:

$$\mu_{\text{Vela}, i} = \int_{E_i^-}^{E_i^+} dE \mathcal{E}(E) E^\Gamma \exp[-(E/E_c)^b], \quad (\text{B.1})$$

and fixed $b = 1$ and $E_c = 3 \text{ GeV}$, which are slightly different than the values reported in ref. [84] for the phase-averaged spectrum.

For the Earth’s limb control sample, we used a phenomenological model to describe the effect of the Earth’s geomagnetic cut-off around 1 GeV on the γ -ray spectrum,

$$\mu_{\text{limb}, i} = \int_{E_i^-}^{E_i^+} dE \mathcal{E}(E) E^{\Gamma_1} [1 + (E/E_b)^{(\Gamma_1 - \Gamma_2)/\beta}]^{-\beta}, \quad (\text{B.2})$$

and fixed $\Gamma_1 = -1.532$, $E_b = 370.3 \text{ MeV}$ and $\beta = 0.7276$. These parameters control the spectrum below the cutoff and the cutoff itself. However, since we limit our fits in the Limb to $E_\gamma > 2 \text{ GeV}$ (above the cutoff), we fix these parameters.

An example of a fit to the Vela pulsar control samples including the signal and background components is shown in figure 9.

The estimates of the fractional residuals from these control samples are shown in figure 9, and are somewhat smaller than from the scan of the Galactic plane. Since the instrumental uncertainties are similar for all the control samples, this suggests that background modelling uncertainties are larger for the control regions in the Galactic plane than for the Vela pulsar and the Earth’s limb. However, notably, from 400 MeV to 2 GeV the results from the Vela pulsar appear to track the results from the Galactic plane control samples, suggesting that these deviations might be caused by a common systematic effect such as energy-dependent variations in the effective area.

²⁰<http://www.atnf.csiro.au/research/pulsar/tempo2/>

²¹<http://fermi.gsfc.nasa.gov/ssc/data/access/lat/ephems/>

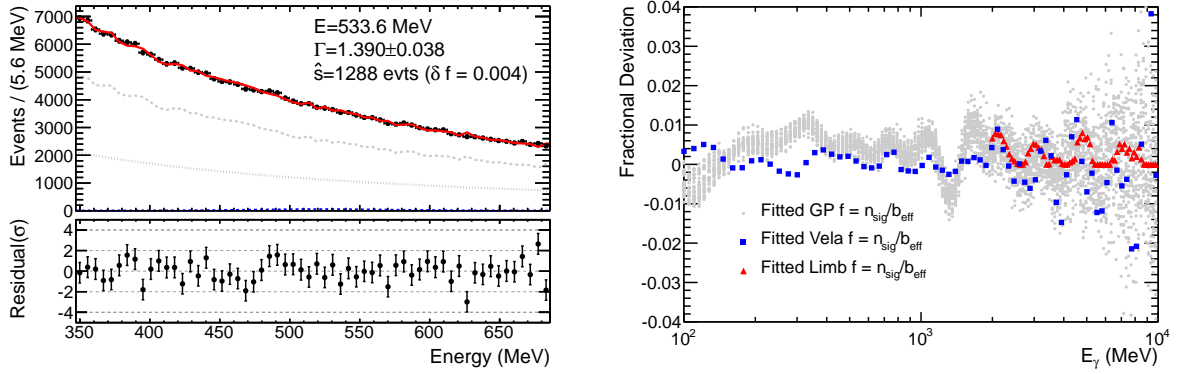


Figure 9. (left) Fit to the Vela pulsar control sample at $E_\gamma = 534$ MeV, showing the models for the off-pulse background (dotted grey line) and the pulsed emission from Vela (dashed grey line); the barely visible dotted blue line shows the signal model. (right) Fractional deviations observed in the Vela pulsar (blue squares), the Earth’s limb (red triangles), and the Galactic plane (GP) scan (grey dots).

C ROI optimisation

As discussed above, the present study is limited by systematic rather than statistical uncertainties. We will hence adopt ROIs that optimise the signal-to-background ratio, rather than the signal-to-noise ratios which is relevant for minimising statistical noise. We note however that we find similar results when considering regions with optimal signal-to-noise ratio. In our search for the best regions, we kept the ROI shape initially identical to the shape used in the high energy line search in ref. [16]. The shape was defined as a circle of radius R_0 centred on the Galactic Centre, excluding part of the disc up to latitude of B_0 while keeping the Galactic Centre in a longitude range $[-L_0, +L_0]$. Namely, we defined the ROIs as the set of points satisfying the following conditions: $(\psi < R_0)$ and $(|b| > B_0 \text{ or } |\ell| < L_0)$, where ψ denotes the angular distance from the Galactic Centre.

We derive the number of expected signal events within the ROI from the baseline Einasto profile in case of both DM annihilation and decay, assuming uniform exposure of the sky. Note that the overall normalisation does not matter for this discussion though the results change very little using the P7REP_CLEAN exposure. We obtain the number of expected background events directly from the distribution of measured γ -rays above 1 GeV (using P7CLEAN data, though the results are very similar using the P7REP_CLEAN data). All three parameters R_0 , B_0 and L_0 are then varied within their physically allowed ranges to find the ROI with maximal signal-to-background ratio, $n_{\text{sig}}/b_{\text{eff}}$. We neglect the impact of the LAT PSF when evaluating n_{sig} . Note that in cases where both signal and background fluxes lack a strong spatial dependence in the relevant regions of the sky, the signal-to-noise ratio, in general, increases with an increasing ROI size. This is not the case for the signal-to-background ratio, where the surface factor cancels out. As a consequence, we do not find very tight constraints on the size of the ROIs. Parameters that yield a very high signal-to-background ratio are in case of DM decay $R_0 = 180^\circ$, $L_0 = 0^\circ$ and $B_0 = 60^\circ$ (we denote this region by ROI_{pol}), and in case of DM annihilation $R_0 = 8^\circ$, $L_0 = 2^\circ$ and $B_0 = 8^\circ$. However, since the signal flux in the second ROI would be severely affected by the broad PSF of the *Fermi*-LAT at very low energies, we selected a simple $20^\circ \times 20^\circ$ ROI around the Galactic Centre instead (ROI_{cen}). We find that this region reduces the signal-to-background ratio by about a factor of two with

respect to the optimal region obtained when PSF effects are neglected.

D Tabulated limits

We provide the flux limits for ROI_{pol} and ROI_{cen} as well as the limits on the decay lifetime and the thermal-averaged annihilation cross-section in tables 3 and 4. These correspond to the limits presented in figures 4 and 5.

E_γ (GeV)	DM Decay – ROI _{pol}				DM Annihilation – ROI _{cen}			
	stat. only		stat. + syst.		stat. only		stat. + syst.	
	ϕ_{mono}	$\tau_{\gamma\nu}$	ϕ_{mono}	$\tau_{\gamma\nu}$	ϕ_{mono}	$\langle\sigma v\rangle_{\gamma\gamma}$	ϕ_{mono}	$\langle\sigma v\rangle_{\gamma\gamma}$
	(cm ⁻² s ⁻¹)	(s)	(cm ⁻² s ⁻¹)	(s)	(cm ⁻² s ⁻¹)	(cm ³ s ⁻¹)	(cm ⁻² s ⁻¹)	(cm ³ s ⁻¹)
	×10 ⁻⁸	×10 ²⁸	×10 ⁻⁸	×10 ²⁸	×10 ⁻⁸	×10 ⁻³⁰	×10 ⁻⁸	×10 ⁻³⁰
0.100	1.04	111	164	0.701	6.71	0.0949	115	1.63
0.110	0.378	276	106	0.988	2.25	0.0386	99.3	1.70
0.121	0.321	296	85.8	1.11	2.70	0.0560	91.7	1.90
0.133	0.369	234	79.2	1.09	6.60	0.166	88.0	2.21
0.146	0.445	177	74.0	1.06	9.00	0.272	82.3	2.49
0.161	1.60	44.7	78.1	0.918	15.2	0.554	80.9	2.95
0.176	16.9	3.87	83.4	0.783	19.2	0.841	78.8	3.45
0.193	18.7	3.20	75.0	0.795	19.6	1.03	73.6	3.88
0.211	18.8	2.89	65.5	0.832	15.3	0.962	64.5	4.07
0.231	10.6	4.71	50.4	0.988	13.6	1.02	58.3	4.40
0.252	5.61	8.13	42.0	1.08	13.1	1.18	54.8	4.94
0.276	6.57	6.36	39.6	1.05	15.2	1.63	55.0	5.91
0.301	12.2	3.14	41.9	0.914	16.8	2.14	54.2	6.93
0.327	12.7	2.77	40.0	0.878	17.4	2.63	52.8	8.00
0.356	8.60	3.75	33.5	0.963	15.5	2.78	48.5	8.71
0.387	2.49	12.0	25.0	1.19	10.3	2.18	40.4	8.55
0.420	1.17	23.4	21.4	1.28	6.85	1.71	34.4	8.58
0.455	2.42	10.5	20.3	1.25	6.66	1.95	31.6	9.24
0.492	2.96	7.89	18.4	1.27	5.47	1.87	27.7	9.49
0.532	3.26	6.63	16.4	1.32	5.23	2.09	25.1	10.0
0.574	2.38	8.41	14.0	1.43	4.56	2.13	22.5	10.5
0.619	1.59	11.7	11.9	1.57	4.60	2.49	20.9	11.3
0.666	2.16	7.99	11.2	1.54	3.46	2.17	18.2	11.4
0.716	3.49	4.61	11.5	1.40	4.52	3.28	17.8	12.9
0.769	2.24	6.68	9.33	1.60	4.33	3.62	16.7	14.0
0.824	1.32	10.6	7.63	1.83	2.33	2.24	13.8	13.3
0.883	0.869	15.0	6.41	2.03	1.46	1.61	11.9	13.1
0.945	0.628	19.4	5.50	2.21	2.35	2.97	11.7	14.8
1.01	0.637	17.9	4.98	2.29	4.17	6.03	12.7	18.4
1.08	0.877	12.1	4.74	2.25	4.54	7.49	12.6	20.8
1.15	0.972	10.3	4.42	2.26	3.19	6.01	9.87	18.6
1.23	0.201	46.6	2.99	3.13	0.319	0.683	5.99	12.8
1.31	0.124	70.7	2.39	3.68	0.0950	0.231	3.96	9.62
1.40	0.216	38.2	2.66	3.10	0.121	0.334	4.13	11.4
1.48	0.698	11.1	3.07	2.53	0.528	1.64	5.33	16.6
1.58	1.07	6.80	3.27	2.23	2.12	7.44	6.75	23.7
1.67	0.761	9.04	2.61	2.63	2.17	8.61	6.09	24.1
1.77	0.695	9.34	2.30	2.82	1.92	8.54	5.63	25.1

Table 3. 95% CL upper limits on γ -ray fluxes, lower limits on DM lifetimes and upper limits on DM annihilation cross sections. We use the Einasto profile to translate flux into lifetime and cross section limits, see appendix A.

E_γ (GeV)	DM Decay – ROI _{pol}					DM Annihilation – ROI _{cen}			
	stat. only		stat. + syst.			stat. only		stat. + syst.	
	ϕ_{mono}	$\tau_{\gamma\nu}$	ϕ_{mono}	$\tau_{\gamma\nu}$		ϕ_{mono}	$\langle\sigma v\rangle_{\gamma\gamma}$	ϕ_{mono}	$\langle\sigma v\rangle_{\gamma\gamma}$
	(cm ⁻² s ⁻¹) ×10 ⁻⁸	(s) ×10 ²⁸	(cm ⁻² s ⁻¹) ×10 ⁻⁸	(s) ×10 ²⁸		(cm ⁻² s ⁻¹) ×10 ⁻⁸	(cm ³ s ⁻¹) ×10 ⁻³⁰	(cm ⁻² s ⁻¹) ×10 ⁻⁸	(cm ³ s ⁻¹) ×10 ⁻³⁰
1.88	0.533	11.5	2.00	3.06		1.63	8.16	4.94	24.7
1.99	0.464	12.5	1.83	3.16		1.19	6.66	4.12	23.1
2.10	0.687	7.96	1.95	2.80		0.853	5.34	3.57	22.3
2.22	0.776	6.68	1.92	2.70		1.17	8.18	3.68	25.6
2.34	0.673	7.30	1.77	2.78		1.39	10.8	3.71	28.8
2.47	0.212	21.9	1.15	4.07		0.923	7.95	2.97	25.6
2.60	0.0913	48.5	0.753	5.88		0.136	1.30	1.72	16.5
2.74	0.123	34.2	0.786	5.35		0.131	1.39	1.59	16.8
2.88	0.432	9.24	1.16	3.45		0.603	7.09	2.17	25.5
3.03	0.712	5.33	1.37	2.77		0.953	12.4	2.32	30.3
3.19	0.421	8.55	1.02	3.54		0.637	9.19	1.86	26.9
3.36	0.347	9.86	0.871	3.93		0.301	4.82	1.40	22.3
3.54	0.195	16.7	0.646	5.04		0.216	3.82	1.20	21.3
3.72	0.0980	31.6	0.457	6.76		0.160	3.14	1.02	20.0
3.91	0.0789	37.3	0.399	7.37		0.325	7.02	1.17	25.4
4.11	0.104	26.9	0.434	6.45		0.505	12.1	1.33	31.8
4.32	0.216	12.3	0.541	4.92		0.467	12.3	1.20	31.6
4.54	0.196	12.9	0.488	5.20		0.532	15.5	1.15	33.4
4.77	0.147	16.4	0.396	6.09		0.482	15.5	1.03	33.2
5.01	0.196	11.7	0.440	5.22		0.408	14.5	0.918	32.6
5.26	0.210	10.4	0.449	4.87		0.273	10.7	0.705	27.6
5.52	0.152	13.7	0.353	5.90		0.108	4.66	0.461	19.9
5.80	0.123	16.1	0.314	6.32		0.0735	3.49	0.369	17.6
6.09	0.107	17.7	0.273	6.93		0.153	8.00	0.488	25.5
6.39	0.167	10.8	0.310	5.80		0.281	16.2	0.599	34.6
6.70	0.295	5.82	0.444	3.87		0.276	17.5	0.547	34.8
7.03	0.301	5.44	0.438	3.74		0.181	12.7	0.407	28.4
7.37	0.0763	20.4	0.188	8.29		0.146	11.2	0.355	27.3
7.73	0.0657	22.6	0.158	9.40		0.174	14.7	0.367	31.0
8.11	0.0812	17.5	0.174	8.16		0.256	23.8	0.473	43.9
8.50	0.153	8.82	0.226	5.99		0.270	27.6	0.421	43.0
8.91	0.116	11.1	0.198	6.51		0.146	16.4	0.271	30.4
9.34	0.0868	14.2	0.170	7.24		0.0810	10.0	0.192	23.7
9.80	0.134	8.78	0.200	5.86		0.0535	7.27	0.158	21.4

Table 4. 95% CL upper limits on γ -ray fluxes, lower limits on DM lifetimes and upper limits on DM annihilation cross sections (continued). We use the Einasto profile to translate flux into lifetime and cross section limits, see appendix A.

References

- [1] Y. Sofue and V. Rubin, *Rotation curves of spiral galaxies*, *Ann.Rev.Astron.Astrophys.* **39** (2001) 137–174, [[astro-ph/0010594](#)].
- [2] **Planck** Collaboration, P. Ade et al., *Planck 2013 results. XVI. Cosmological parameters*, [arXiv:1303.5076](#).
- [3] C. Muñoz, *Dark matter detection in the light of recent experimental results*, *Int.J.Mod.Phys.* **A19** (2004) 3093–3170, [[hep-ph/0309346](#)].
- [4] G. Bertone, D. Hooper, and J. Silk, *Particle dark matter: Evidence, candidates and constraints*, *Phys.Rept.* **405** (2005) 279–390, [[hep-ph/0404175](#)].
- [5] L. Bergström, *Dark Matter Evidence, Particle Physics Candidates and Detection Methods*, *Annalen Phys.* **524** (2012) 479–496, [[arXiv:1205.4882](#)].
- [6] G. Servant and T. M. Tait, *Is the lightest Kaluza-Klein particle a viable dark matter candidate?*, *Nucl.Phys.* **B650** (2003) 391–419, [[hep-ph/0206071](#)].
- [7] H.-C. Cheng, J. L. Feng, and K. T. Matchev, *Kaluza-Klein dark matter*, *Phys.Rev.Lett.* **89** (2002) 211301, [[hep-ph/0207125](#)].
- [8] D. G. Cerdeño, C. Muñoz, and O. Seto, *Right-handed sneutrino as thermal dark matter*, *Phys.Rev.* **D79** (2009) 023510, [[arXiv:0807.3029](#)].
- [9] D. G. Cerdeño, M. Peiro, and S. Robles, *Low-mass right-handed sneutrino dark matter: SuperCDMS and LUX constraints and the Galactic Centre gamma-ray excess*, [arXiv:1404.2572](#).
- [10] K.-Y. Choi, D. E. López-Fogliani, C. Muñoz, and R. R. de Austri, *Gamma-ray detection from gravitino dark matter decay in the $\mu\nu$ SSM*, *JCAP* **1003** (2010) 028, [[arXiv:0906.3681](#)].
- [11] **Fermi-LAT** Collaboration, W. Atwood et al., *The Large Area Telescope on the Fermi Gamma-ray Space Telescope Mission*, *Astrophys.J.* **697** (2009) 1071–1102, [[arXiv:0902.1089](#)].
- [12] S. Funk, *Indirect Detection of Dark Matter with gamma rays*, [arXiv:1310.2695](#).
- [13] **Fermi-LAT** Collaboration, A. Abdo et al., *Fermi LAT Search for Photon Lines from 30 to 200 GeV and Dark Matter Implications*, *Phys.Rev.Lett.* **104** (2010) 091302, [[arXiv:1001.4836](#)].
- [14] G. Vertongen and C. Weniger, *Hunting Dark Matter Gamma-Ray Lines with the Fermi LAT*, *JCAP* **1105** (2011) 027, [[arXiv:1101.2610](#)].
- [15] **Fermi-LAT** Collaboration, M. Ackermann et al., *Fermi LAT Search for Dark Matter in Gamma-ray Lines and the Inclusive Photon Spectrum*, *Phys.Rev.* **D86** (2012) 022002, [[arXiv:1205.2739](#)].
- [16] **Fermi-LAT** Collaboration, M. Ackermann et al., *Search for Gamma-ray Spectral Lines with the Fermi Large Area Telescope and Dark Matter Implications*, *Phys.Rev.* **D88** (2013) 082002, [[arXiv:1305.5597](#)].
- [17] C. Weniger, *A Tentative Gamma-Ray Line from Dark Matter Annihilation at the Fermi Large Area Telescope*, *JCAP* **1208** (2012) 007, [[arXiv:1204.2797](#)].
- [18] S. P. Martin, *A Supersymmetry primer*, [hep-ph/9709356](#).
- [19] J. E. Kim and H. P. Nilles, *The μ Problem and the Strong CP Problem*, *Phys.Lett.* **B138** (1984) 150.
- [20] D. López-Fogliani and C. Muñoz, *Proposal for a supersymmetric standard model*, *Phys.Rev.Lett.* **97** (2006) 041801, [[hep-ph/0508297](#)].
- [21] N. Escudero, D. E. López-Fogliani, C. Muñoz, and R. R. de Austri, *Analysis of the parameter space and spectrum of the $\mu\nu$ SSM*, *JHEP* **0812** (2008) 099, [[arXiv:0810.1507](#)].

- [22] P. Ghosh and S. Roy, *Neutrino masses and mixing, lightest neutralino decays and a solution to the μ problem in supersymmetry*, *JHEP* **0904** (2009) 069, [[arXiv:0812.0084](#)].
- [23] A. Bartl, M. Hirsch, A. Vicente, S. Liebler, and W. Porod, *LHC phenomenology of the $\mu\nu$ SSM*, *JHEP* **0905** (2009) 120, [[arXiv:0903.3596](#)].
- [24] J. Fidalgo, D. E. López-Fogliani, C. Muñoz, and R. Ruiz de Austri, *Neutrino Physics and Spontaneous CP Violation in the $\mu\nu$ SSM*, *JHEP* **0908** (2009) 105, [[arXiv:0904.3112](#)].
- [25] P. Ghosh, P. Dey, B. Mukhopadhyaya, and S. Roy, *Radiative contribution to neutrino masses and mixing in $\mu\nu$ SSM*, *JHEP* **1005** (2010) 087, [[arXiv:1002.2705](#)].
- [26] J. Fidalgo, D. E. López-Fogliani, C. Muñoz, and R. R. de Austri, *The Higgs sector of the $\mu\nu$ SSM and collider physics*, *JHEP* **1110** (2011) 020, [[arXiv:1107.4614](#)].
- [27] P. Bandyopadhyay, P. Ghosh, and S. Roy, *Unusual Higgs boson signal in R-parity violating nonminimal supersymmetric models at the LHC*, *Phys.Rev.* **D84** (2011) 115022, [[arXiv:1012.5762](#)].
- [28] S. Liebler and W. Porod, *On-shell renormalization of neutralino and chargino mass matrices in R-parity violating models - Correlation between LSP decays and neutrino mixing angles revisited*, *Nucl.Phys.* **B855** (2012) 774–800, [[arXiv:1106.2921](#)].
- [29] P. Ghosh, D. E. López-Fogliani, V. A. Mitsou, C. Muñoz, and R. Ruiz de Austri, *Probing the μ from ν supersymmetric standard model with displaced multileptons from the decay of a Higgs boson at the LHC*, *Phys.Rev.* **D88** (2013) 015009, [[arXiv:1211.3177](#)].
- [30] P. Ghosh, D. E. Lopez-Fogliani, V. A. Mitsou, C. Muñoz, and R. R. de Austri, *Hunting physics beyond the standard model with unusual W^\pm and Z decays*, [arXiv:1403.3675](#).
- [31] D. J. Chung and A. J. Long, *Electroweak Phase Transition in the $\mu\nu$ SSM*, *Phys.Rev.* **D81** (2010) 123531, [[arXiv:1004.0942](#)].
- [32] Y. Farzan and J. Valle, *R-parity violation assisted thermal leptogenesis in the seesaw mechanism*, *Phys.Rev.Lett.* **96** (2006) 011601, [[hep-ph/0509280](#)].
- [33] F. Takayama and M. Yamaguchi, *Gravitino dark matter without R-parity*, *Phys.Lett.* **B485** (2000) 388–392, [[hep-ph/0005214](#)].
- [34] W. Buchmüller, L. Covi, K. Hamaguchi, A. Ibarra, and T. Yanagida, *Gravitino Dark Matter in R-Parity Breaking Vacua*, *JHEP* **0703** (2007) 037, [[hep-ph/0702184](#)].
- [35] S. Lola, P. Osland, and A. Raklev, *Radiative gravitino decays from R-parity violation*, *Phys.Lett.* **B656** (2007) 83–90, [[arXiv:0707.2510](#)].
- [36] M. A. Díaz, S. G. Sáenz, and B. Koch, *Gravitino Dark Matter and Neutrino Masses in Partial Split Supersymmetry*, *Phys.Rev.* **D84** (2011) 055007, [[arXiv:1106.0308](#)].
- [37] D. Restrepo, M. Taoso, J. Valle, and O. Zapata, *Gravitino dark matter and neutrino masses with bilinear R-parity violation*, *Phys.Rev.* **D85** (2012) 023523, [[arXiv:1109.0512](#)].
- [38] A. Ibarra and D. Tran, *Gamma Ray Spectrum from Gravitino Dark Matter Decay*, *Phys.Rev.Lett.* **100** (2008) 061301, [[arXiv:0709.4593](#)].
- [39] H.-B. Kim and J. E. Kim, *Late decaying axino as CDM and its lifetime bound*, *Phys.Lett.* **B527** (2002) 18–22, [[hep-ph/0108101](#)].
- [40] L. Covi and J. E. Kim, *Axinos as Dark Matter Particles*, *New J.Phys.* **11** (2009) 105003, [[arXiv:0902.0769](#)].
- [41] **Fermi-LAT** Collaboration, A. Abdo et al., *Fermi Large Area Telescope Measurements of the Diffuse Gamma-Ray Emission at Intermediate Galactic Latitudes*, *Phys.Rev.Lett.* **103** (2009) 251101, [[arXiv:0912.0973](#)].

- [42] G. Gómez-Vargas, M. Fornasa, F. Zandanel, A. Cuesta, C. Muñoz, et al., *CLUES on Fermi-LAT prospects for the extragalactic detection of $\mu\nu$ SSM gravitino Dark Matter*, *JCAP* **1202** (2012) 001, [[arXiv:1110.3305](#)].
- [43] A. R. Pullen, R.-R. Chary, and M. Kamionkowski, *Search with EGRET for a Gamma Ray Line from the Galactic Center*, *Phys.Rev.* **D76** (2007) 063006, [[astro-ph/0610295](#)].
- [44] K. Ishiwata, S. Matsumoto, and T. Moroi, *High Energy Cosmic Rays from the Decay of Gravitino Dark Matter*, *Phys.Rev.* **D78** (2008) 063505, [[arXiv:0805.1133](#)].
- [45] K.-Y. Choi, D. Restrepo, C. E. Yaguna, and O. Zapata, *Indirect detection of gravitino dark matter including its three-body decays*, *JCAP* **1010** (2010) 033, [[arXiv:1007.1728](#)].
- [46] M. A. Díaz, S. G. Sáenz, and B. Koch, *Gravitino Dark Matter and Neutrino Masses in Partial Split Supersymmetry*, *Phys.Rev.* **D84** (2011) 055007, [[arXiv:1106.0308](#)].
- [47] M. Grefe, *Unstable Gravitino Dark Matter - Prospects for Indirect and Direct Detection*, *DESY-THESIS-2011-039* (2011) [[arXiv:1111.6779](#)].
- [48] L. Covi, M. Grefe, A. Ibarra, and D. Tran, *Unstable Gravitino Dark Matter and Neutrino Flux*, *JCAP* **0901** (2009) 029, [[arXiv:0809.5030](#)].
- [49] D. Forero, M. Tortola, and J. Valle, *Global status of neutrino oscillation parameters after Neutrino-2012*, *Phys.Rev.* **D86** (2012) 073012, [[arXiv:1205.4018](#)].
- [50] M. González-García, M. Maltoni, J. Salvado, and T. Schwetz, *Global fit to three neutrino mixing: critical look at present precision*, *JHEP* **1212** (2012) 123, [[arXiv:1209.3023](#)].
- [51] J. R. Ellis, A. D. Linde, and D. V. Nanopoulos, *Inflation Can Save the Gravitino*, *Phys.Lett.* **B118** (1982) 59.
- [52] J. Pradler and F. D. Steffen, *Thermal gravitino production and collider tests of leptogenesis*, *Phys.Rev.* **D75** (2007) 023509, [[hep-ph/0608344](#)].
- [53] J. Pradler and F. D. Steffen, *Constraints on the Reheating Temperature in Gravitino Dark Matter Scenarios*, *Phys.Lett.* **B648** (2007) 224–235, [[hep-ph/0612291](#)].
- [54] **Particle Data Group** Collaboration, J. Beringer et al., *Review of Particle Physics (RPP)*, *Phys.Rev.* **D86** (2012) 010001.
- [55] M. Bolz, A. Brandenburg, and W. Buchmüller, *Thermal production of gravitinos*, *Nucl.Phys.* **B606** (2001) 518–544, [[hep-ph/0012052](#)].
- [56] H. Pagels and J. R. Primack, *Supersymmetry, Cosmology and New TeV Physics*, *Phys.Rev.Lett.* **48** (1982) 223.
- [57] **ATLAS** Collaboration, J. Boyd, “Overview of SUSY results from the ATLAS experiment.” talk given at the SUSY 2013 conference, ICTP Trieste, Italy, 26–31 August 2013, https://atlas.web.cern.ch/Atlas/GROUPS/PHYSICS/CombinedSummaryPlots/SUSY/ATLAS_SUSY_Summary/ATLAS_SUSY_Summary.pdf.
- [58] **CMS** Collaboration, J. Richman, “Searches for Supersymmetry in the CMS Experiment.” talk given at the SUSY 2013 conference, ICTP Trieste, Italy, 26–31 August 2013, https://twiki.cern.ch/twiki/pub/CMSPublic/SUSYSMSSummaryPlots8TeV/barplot_blue_orange_SUSY2013.pdf.
- [59] M. Viel, J. Lesgourgues, M. G. Haehnelt, S. Matarrese, and A. Riotto, *Constraining warm dark matter candidates including sterile neutrinos and light gravitinos with WMAP and the Lyman-alpha forest*, *Phys.Rev.* **D71** (2005) 063534, [[astro-ph/0501562](#)].
- [60] M. Viel, G. D. Becker, J. S. Bolton, M. G. Haehnelt, M. Rauch, et al., *How cold is cold dark matter? Small scales constraints from the flux power spectrum of the high-redshift Lyman-alpha forest*, *Phys.Rev.Lett.* **100** (2008) 041304, [[arXiv:0709.0131](#)].

- [61] S. Hannestad, *What is the lowest possible reheating temperature?*, *Phys.Rev.* **D70** (2004) 043506, [[astro-ph/0403291](#)].
- [62] M. Fukugita and T. Yanagida, *Baryogenesis Without Grand Unification*, *Phys.Lett.* **B174** (1986) 45.
- [63] M. Kawasaki, K. Kohri, T. Moroi, and A. Yotsuyanagi, *Big-Bang Nucleosynthesis and Gravitino*, *Phys.Rev.* **D78** (2008) 065011, [[arXiv:0804.3745](#)].
- [64] A. Ghez, S. Salim, N. Weinberg, J. Lu, T. Do, et al., *Measuring Distance and Properties of the Milky Way’s Central Supermassive Black Hole with Stellar Orbits*, *Astrophys.J.* **689** (2008) 1044–1062, [[arXiv:0808.2870](#)].
- [65] S. Gillessen, F. Eisenhauer, S. Trippe, T. Alexander, R. Genzel, et al., *Monitoring stellar orbits around the Massive Black Hole in the Galactic Center*, *Astrophys.J.* **692** (2009) 1075–1109, [[arXiv:0810.4674](#)].
- [66] R. Catena and P. Ullio, *A novel determination of the local dark matter density*, *JCAP* **1008** (2010) 004, [[arXiv:0907.0018](#)].
- [67] J. Einasto, *On the Construction of a Composite Model for the Galaxy and on the Determination of the System of Galactic Parameters*, *Trudy Astrofizicheskogo Instituta Alma-Ata* **5** (1965) 87–100.
- [68] J. F. Navarro, E. Hayashi, C. Power, A. Jenkins, C. S. Frenk, et al., *The Inner structure of Lambda-CDM halos 3: Universality and asymptotic slopes*, *Mon.Not.Roy.Astron.Soc.* **349** (2004) 1039, [[astro-ph/0311231](#)].
- [69] M. Weber and W. de Boer, *Determination of the Local Dark Matter Density in our Galaxy*, *Astron.Astrophys.* **509** (2010) A25, [[arXiv:0910.4272](#)].
- [70] P. Salucci, F. Nesti, G. Gentile, and C. Martins, *The dark matter density at the Sun’s location*, *Astron.Astrophys.* **523** (2010) A83, [[arXiv:1003.3101](#)].
- [71] **Fermi-LAT** Collaboration, M. Ackermann et al., *The Fermi Large Area Telescope On Orbit: Event Classification, Instrument Response Functions, and Calibration*, *Astrophys.J.Suppl.* **203** (2012) 4, [[arXiv:1206.1896](#)].
- [72] T. Bringmann, X. Huang, A. Ibarra, S. Vogl, and C. Weniger, *Fermi LAT Search for Internal Bremsstrahlung Signatures from Dark Matter Annihilation*, *JCAP* **1207** (2012) 054, [[arXiv:1203.1312](#)].
- [73] W. A. Rolke, A. M. Lopez, and J. Conrad, *Limits and confidence intervals in the presence of nuisance parameters*, *Nucl.Instrum.Meth.* **A551** (2005) 493–503, [[physics/0403059](#)].
- [74] W. Verkerke and D. P. Kirkby, *The RooFit toolkit for data modeling*, *eConf* **C0303241** (2003) MOLT007, [[physics/0306116](#)].
- [75] J. F. Navarro, C. S. Frenk, and S. D. White, *The Structure of cold dark matter halos*, *Astrophys.J.* **462** (1996) 563–575, [[astro-ph/9508025](#)].
- [76] J. N. Bahcall and R. Soneira, *The Universe at faint magnetitudes. 2. Models for the predicted star counts*, *Astrophys.J.Suppl.* **44** (1980) 73–110.
- [77] A. Burkert, *The Structure of dark matter halos in dwarf galaxies*, *IAU Symp.* **171** (1996) 175, [[astro-ph/9504041](#)].
- [78] F. Nesti and P. Salucci, *The Dark Matter halo of the Milky Way, AD 2013*, *JCAP* **1307** (2013) 016, [[arXiv:1304.5127](#)].
- [79] M. Cirelli, G. Corcella, A. Hektor, G. Hutsi, M. Kadastik, et al., *PPPC 4 DM ID: A Poor Particle Physicist Cookbook for Dark Matter Indirect Detection*, *JCAP* **1103** (2011) 051, [[arXiv:1012.4515](#)].

- [80] F. Iocco, M. Pato, G. Bertone, and P. Jetzer, *Dark Matter distribution in the Milky Way: microlensing and dynamical constraints*, *JCAP* **1111** (2011) 029, [[arXiv:1107.5810](#)].
- [81] G. A. Gómez-Vargas, M. A. Sanchez-Conde, J.-H. Huh, M. Peiro, F. Prada, et al., *Constraints on WIMP Annihilation for Contracted Dark Matter in the Inner Galaxy with the Fermi-LAT*, *JCAP* **1310** (2013) 029, [[arXiv:1308.3515](#)].
- [82] D. P. Finkbeiner, M. Su, and C. Weniger, *Is the 130 GeV Line Real? A Search for Systematics in the Fermi-LAT Data*, *JCAP* **1301** (2013) 029, [[arXiv:1209.4562](#)].
- [83] G. Hobbs, R. Edwards, and R. Manchester, *Tempo2, a new pulsar timing package. 1. overview*, *Mon.Not.Roy.Astron.Soc.* **369** (2006) 655–672, [[astro-ph/0603381](#)].
- [84] **Fermi-LAT** Collaboration, A. Abdo, *The Vela Pulsar: Results from the First Year of Fermi LAT Observations*, *Astrophys.J.* **713** (2010) 154–165, [[arXiv:1002.4050](#)].
- [85] P. Weltevrede, S. Johnston, R. Manchester, R. Bhat, M. Burgay, et al., *Pulsar Timing with the Parkes Radio Telescope for the Fermi Mission*, [arXiv:0909.5510](#).